AD-A146 539 AN INVESTIGATION OF THE ELECTRICAL CONDUCTIVITY IN HIGHLY ORIENTED GRAPHI..(U) MOORE SCHOOL OF ELECTRICAL ENGINEERING PHILADELPHIA PA DEPT O.. F L VOGEL FEB 84 1/2

UNCLASSIFIED DAAG53-76-C-0061 F/G 11/2 NL

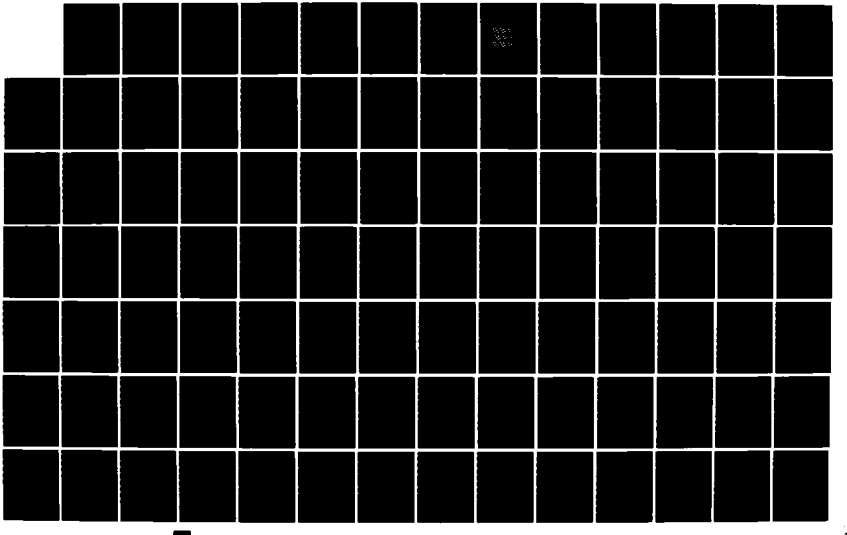

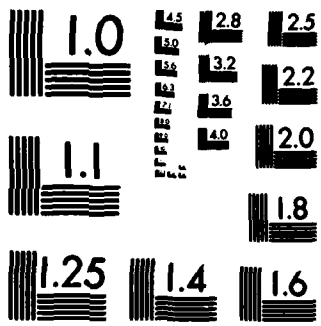

UNCLASSIFIED

SECURITY CLASSIFICATION OF THIS PAGE (When Data Entered)

REPORT DOCUMENTATION PAGE

READ INSTRUCTIONS BEFORE COMPLETING FORM

1. REPORT NUMBER

2. GOVT ACCESSION NO.

3. RECIPIENT'S CATALOG NUMBER

4. TITLE (and Subtitle)
FINAL REPORT on An Investigation of the Electrical Conductivity in Highly Oriented Graphite Intercalation Compounds

5. TYPE OF REPORT & PERIOD COVERED
Final

6. PERFORMING ORG. REPORT NUMBER

7. AUTHOR(s)
F. Lincoln Vogel

8. CONTRACT OR GRANT NUMBER(s)
DAAG53-76-C-0061

9. PERFORMING ORGANIZATION NAME AND ADDRESS
University of Pennsylvania
Department of Electrical Engineering
Philadelphia, PA 19104

10. PROGRAM ELEMENT, PROJECT, TASK AREA & WORK UNIT NUMBERS
1L161102AH51-PA

11. CONTROLLING OFFICE NAME AND ADDRESS
Mobility Equipment Research & Development Command
DRDME-EAC, Fort Belvoir, Virginia 22060-5606

12. REPORT DATE
February 1984

13. NUMBER OF PAGES
113

14. MONITORING AGENCY NAME & ADDRESS(if different from Controlling Office)
Mobility Equipment Research and Development Command
Ft. Belvoir, Virginia 22060-5606

15. SECURITY CLASS. (of this report)
UNCLASSIFIED

15a. DECLASSIFICATION/DOWNGRADING SCHEDULE

16. DISTRIBUTION STATEMENT (of this Report)
Distribution unlimited.

This document has been approved for public release and sale; its distribution is unlimited.

17. DISTRIBUTION STATEMENT (of the abstract entered in Block 20, if different from Report)

18. SUPPLEMENTARY NOTES

1 1 1984

A

19. KEY WORDS (Continue on reverse side if necessary and identify by block number)
Graphite
Intercalation Compounds
Synthetic Metals
Antimony Pentafluoride
Arsenic Pentafluoride

20. ABSTRACT (Continue on reverse side if necessary and identify by block number)
It was the possibility of making a lightweight, practical conductor of electricity that led to the research reported here. Pristine graphite consists of carbon atoms arranged in a hexagonal layered structure as shown in Fig. 1. It is a semi metal with room temperature a axis resistivity about 23 times higher than copper (1). The weak bonding forces between the layers allow various atomic and molecular species to be interstitially inserted or intercalated as

DD FORM 1 JAN 73 1473 EDITION OF 1 NOV 65 IS OBSOLETE

UNCLASSIFIED

SECURITY CLASSIFICATION OF THIS PAGE (When Data Entered)

ENCL 1

shown in Figure 2, for the case of a potassium intercalation compound. There is an exchange of electrons between the graphite host lattice and the intercalant which increases the carrier concentration in the latter causing graphite intercalation compounds (GICs) to have metallic properties, including substantially higher electrical conductivities than pristine graphite.

The high degree of order associated with GICs leads to the characterization of the compounds by staging. The stage of a compound refers to the number of graphite layers between each two layers of intercalant as shown in Figure 3.

SbF_5, which acts as an acceptor in GICs has been observed to yield compounds having a axis conductivity comparable to that of copper (3). The following is a report of an extensive investigation of the various aspects of SbF_5 intercalated graphite of interest to its use as a practical conductor.

Section II deals with an IR re-investigation of SbF_5 intercalated graphite powder in an effort to expose a possible fluoride constituent (CF?) which may contribute to a reduced electrical conductivity. Section III describes an effort to repeat an earlier successful experiment producing high conductivity swaged wires. Section IV deals with the fundamental conduction properties of polycrystalline SbF_5-intercalated graphite and Section V reports a basic investigation of the conduction mechanisms in SbF_5 intercalated graphite crystal as influenced by temperature and structural changes. In totality these investigations were conducted to provide a better understanding of electrical conduction of graphite intercalated with a typical acceptor of the strong Lewis acid type to better apply these materials as practical conductors.

Earlier work under this contract has been reported in "An Investigation of the Electrical Conductivity in Highly Anisotropic Graphite Intercalation Compounds, Dec. 9, 1975 - Jan. 23, 1978," by F.L. Vogel, J. Gan and T.C. Wu (11); "Electrical Transport Properties of Graphite Intercalated with Antimony Pentafloride", by T.C. Wu (2); "Assuaging Desire for Swaging the Wire," by S. Mendelsohn (49); which are incorporated by reference.

UNIVERSITY OF PENNSYLVANIA
THE MOORE SCHOOL OF ELECTRICAL ENGINEERING
PHILADELPHIA, PA 19104

Final Report on

An Investigation of the Electrical Conductivity in Highly Oriented Graphite Intercalation Compounds

Contract No. DAAG53-76-C-0061

to

Mobility Equipment Research and Development Command
Ft. Belvoir, Virginia 20060

Principal Investigator: F. Lincoln Vogel

A-1

TABLE OF CONTENTS

TABLE OF CONTENTS (cont)

I. General Introduction

It was the possibility of making a lightweight, practical conductor of electricity that led to the research reported here. Pristine graphite consists of carbon atoms arranged in a hexagonal layered structure as shown in Figure 1. It is a semi metal with room temperature a axis resistivity about 23 times higher than copper (1). The weak bonding forces between the layers allow various atomic and molecular species to be interstitially inserted or intercalated as shown in Figure 2 for the case of a potassium intercalation compound. There is an exchange of electrons between the graphite host lattice and the intercalant which increases the carrier concentration in the latter causing graphite intercalation compounds (GICs) to have metallic properties, including substantially higher electrical conductivities than pristine graphite.

The high degree of order associated with GICs leads to the characterization of the compounds by staging. The stage of a compound refers to the number of graphite layers between each two layers of intercalant as shown in Figure 3.

SbF_5, which acts as an acceptor in GICs has been observed to yield compounds having a axis conductivity comparable to that of copper (3). The following is a report of an extensive investigation of the various aspects of SbF_5 intercalated graphite of interest to its use as a practical conductor.

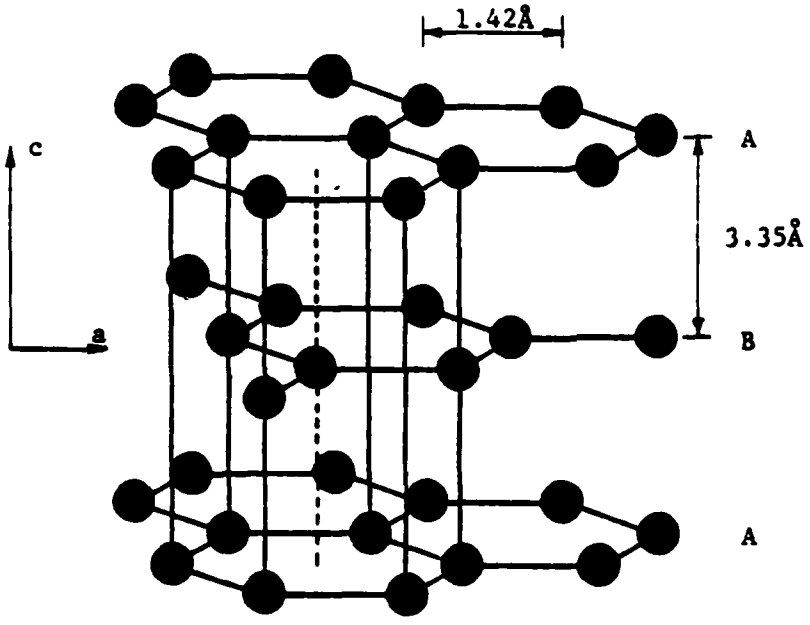

Figure 1. Crystal structure of graphite.[2]

Section II deals with an IR re-investigation of SbF_5 intercalated graphite powder in an effort to expose a possible fluoride constituent (CF?) which may contribute to a reduced electrical conductivity. Section III describes an effort to repeat an earlier successful experiment producing high conductivity swaged wires. Section IV deals with the fundamental conduction properties of polycrystalline SbF_5-intercalated graphite and Section V reports a basic investigation of the conduction mechanisms in SbF_5 intercalated graphite crystal as influenced by temperature and structural changes. In totality these investigations were conducted to provide a better understanding of electrical conduction of graphite intercalated with a typical acceptor of the strong Lewis acid type to better apply these materials as practical conductors.

Earlier work under this contract has been reported in "An Investigation of the Electrical Conductivity in Highly Anisotropic Graphite Intercalation Compounds, Dec. 9, 1975 - Jan. 23, 1978," by F.L. Vogel, J. Gan and T.C. Wu (11); "Electrical Transport Properties of Graphite Intercalated with Antimony Pentafloride", by T.C. Wu (2); "Assuaging Desire for Swaging the Wire," by S. Mendelsohn (49); which are incorporated by reference.

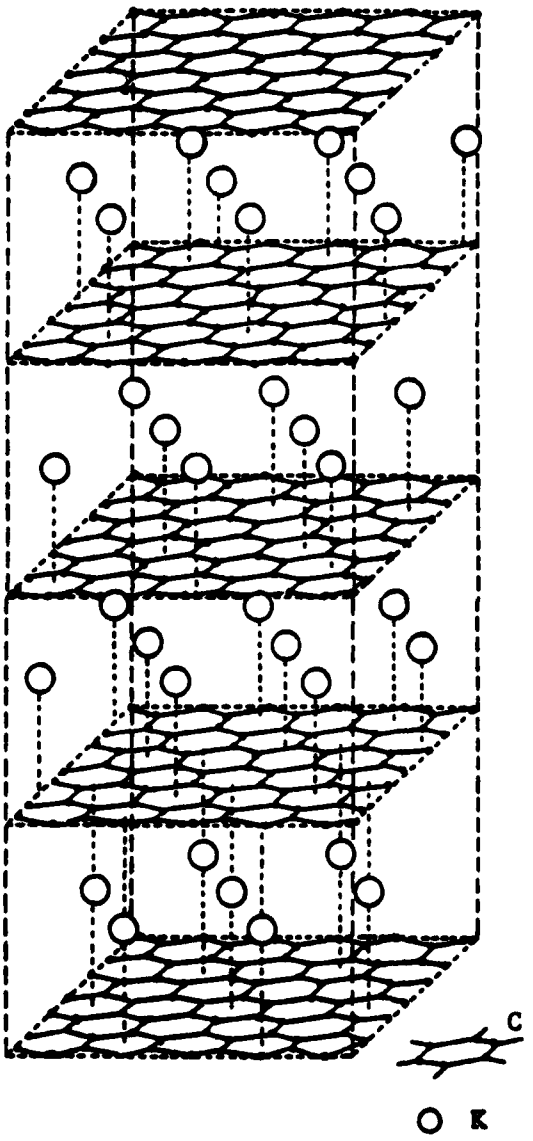

Figure 2. Crystal structure of potassium graphite, C_8K.[4]

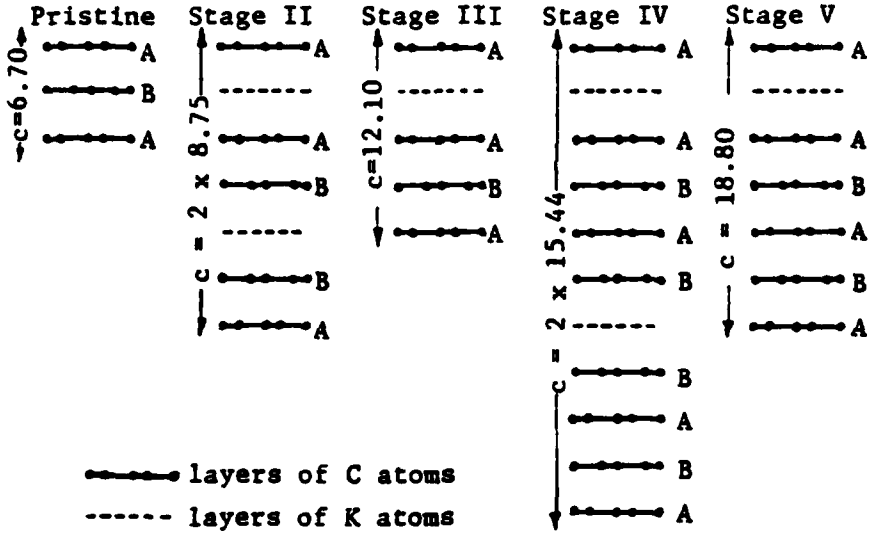

Figure 3. Sequences of carbon hexagon networks and potassium atoms in various compounds, viewed perpendicular to the c-axis.[4]

II. Investigation of Intercalated Graphite by Infrared Spectroscopy

A. Introduction

The conductivity σ of a material can be expressed by the equation $\sigma = ne\mu$ where n is the carrier concentration, be it by electrons or holes; e is the electron charge; and μ is the mobility of those carriers in that material. Anything that diminished either the concentration or mobility naturally has a deleterious effect on the material's conductivity. It is possible that carbon fluorination of graphite intercalated with antimony pentafluoride (SbF_5) inhibits conductivity by reducing both carrier concentration and mobility by the following reaction.

$$C_n + SbF_6^- \longrightarrow CF + C_{n-1} + SbF_5.$$ [5]

Evidence of this carbon fluorination was reported to have been seen in infrared spectra of intercalated powders.[6] In an attempt at replicating these results, the same KBr matrix technique was employed using SbF_5 intercalated graphite.

B. Preparation of SbF_5 Intercalated Graphite Powders

A teflon ampoule (Figure 4) is filled with a known weight of pristine graphite powder (in this case, Superior #2135). The ampoule is placed in a vacuum oven with its lid unscrewed. The powder is baked ($\sim$150°C) and pumped on overnight to remove adsorbed water. The oven is then purged with an inert gas (e.g.argon) and the lid is quickly screwed on and hand tightened. The ampoule is removed to an inert atmosphere glove box, where the appropriate amount of SbF_5 liquid is added using a pipette and rubber bulb. From T.C. Wu's results[2] and the known densities of SbF_5 and graphite, one can calculate the necessary mixing proportions to insure the desired staging. See Table 1.

Once the SbF_5 has been added to the graphite, the ampoule is sealed and tightened gently with a wrench to insure air-tightness. The ampoule may be placed on a mixer mill or a roller for a period of time to allow mixing of the liquid and powder. After mixing, the ampoule is baked in an oven at $\sim$150 C for a few days.

C. Characterization of Graphite Powders

In order to characterize the powder in terms of stage, an X-ray spectrum is taken. In the glove box, a small amount of powder is placed in a .5 mm glass capillary tube (Charles

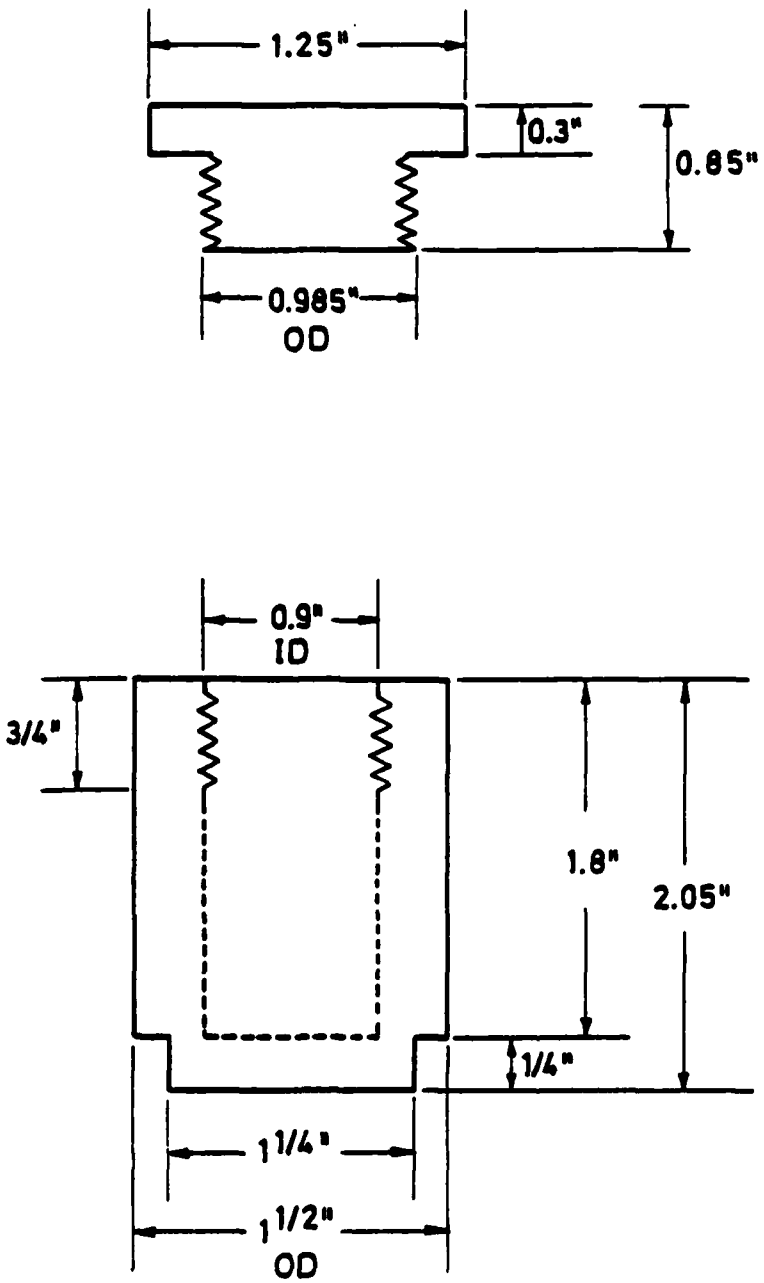

Figure 4. Teflon ampoule used for intercalating graphite powder.

Table 1. Mixing proportions for SbF_5 intercalated graphite.[2]

Stage	m in C_mSbF_5	Volume SbF_5 per gm graphite
I	8.5-9.0	.69 ml
II	18	.33
III	27	.22
IV	35	.17

Supper Co.). A fine steel wire is used to pack the powder gently to the bottom of the capillary tube. After sealing the top of the tube with silicon stopcock grease, it can be removed from the glove box for permanent sealing. This is done using a match or low gas flame to melt the glass just above the graphite level to give a sample about one half inch long.

The powder sample is placed in a camera for Debye-Scherrer X-ray diffraction. After exposure and development of the film, the spectrum is analyzed and the powder is characterized using the d-spacing information gathered. The d-spacing for SbF_5 intercalated graphite can be found in T.C.Wu's thesis.[2]

D. Preparation of KBr Matrix Pellets

In order to run an IR spectroscopy experiment on an air-sensitive material like SbF_5 intercalated graphite, the KBr matrix method is employed. The method involves the preparation of a pressed mixture of KBr and graphite sandwiched between two layers of KBr. KBr is transparent in the IR spectrum and provides a combination window, support, and protective seal for the graphite compound.

The first step in this method is the same as in the preparation of intercalated powders; that is, the drying out of the KBr in a vacuum oven. Once the KBr is dried and moved into an inert glove box atmosphere, the matrix is constructed using either of two die arrangements (Figures 5 and 6). Using an onyx mortar and pestle, the KBr is mashed and ground to a fine white powder; the finer the better.

The first layer is made by pressing $\sim$ 50 mg of KBr in the die forming a clear crystal sheet covering the entire die cross-section. A mixture of intercalated powder and crushed KBr is prepared using 1-7 mg of graphite per 100 mg of KBr. About 100 mg of this mixture is added to the die and pressed right on top of the first layer to form the middle of the matrix. The sample is completed by adding another 50 mg of KBr to form the other protective layer of the pellet.

Removing both bolts and leaving the pellet intact in the die, the sample is taken immediately to the spectrometer (Perkin-Elmer 224 grating model) and the IR spectrum is recorded.

IR spectroscopy measures absorbance vs. wavelength. The spectra show troughs which correspond to those wavelengths at which absorption occurs. The frequency of these troughs correspond to the normal vibrational modes of the chemical

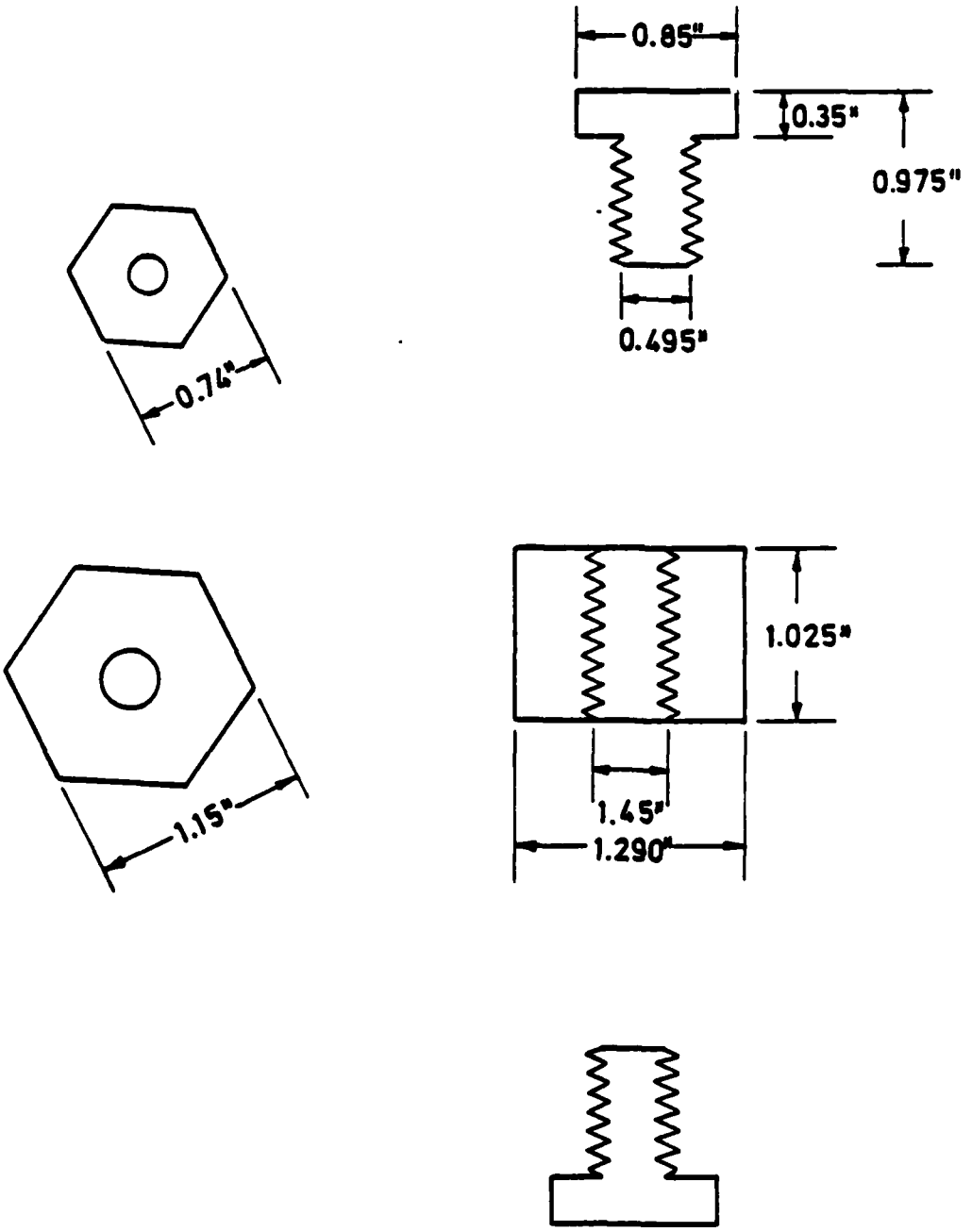

Figure 5. Die for preparing KBr matrices; arrangement A.

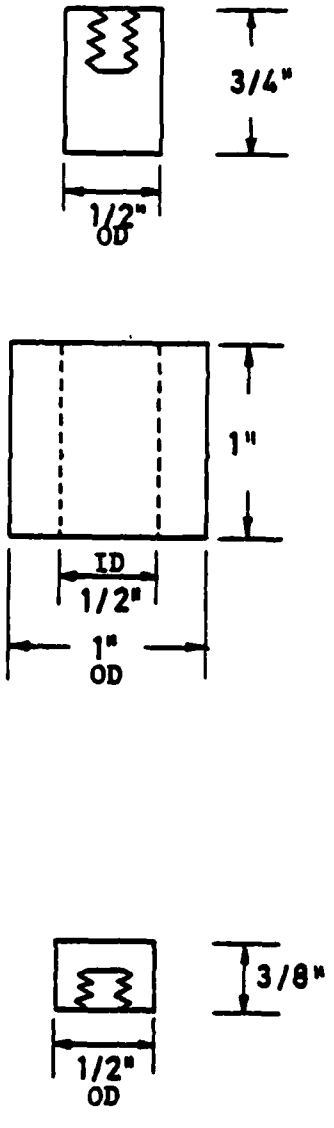

Figure 6. Die for preparing KBr matrices; arrangement B.

species present. Radiation with a frequency corresponding to a normal mode is absorbed and either re-radiated in a random direction or degenerated as heat. In either case, the result is a lower transmission level for that frequency compared to the other frequencies that do not interact. This leads to the characteristic troughs in the IR spectrum.

E. Experimental Procedures

The first spectra taken were of pellets made entirely out of KBr, both dried and undried, to get a working reference (see Figure 7). The trough here corresponds to a KNO_3 impurity in the KBr. Pellets were prepared using SbF_5 compounds of stages I and II. A pellet was also prepared mixing KBr with some small clear crystals that were found growing in the ampoule of the stage I powder.

F. Results and Discussion

The first problem encountered was in preparing a pellet which had the proper graphite-to-KBr ratio. If too much graphite is used in the mixture or indeed if too much of the mixture itself is used, the transmission of IR radiation through the pellet will be too low to yield any reasonable sensitivity to absorption peaks anywhere in the range. On the other hand, if the sample mixture is too dilute, the

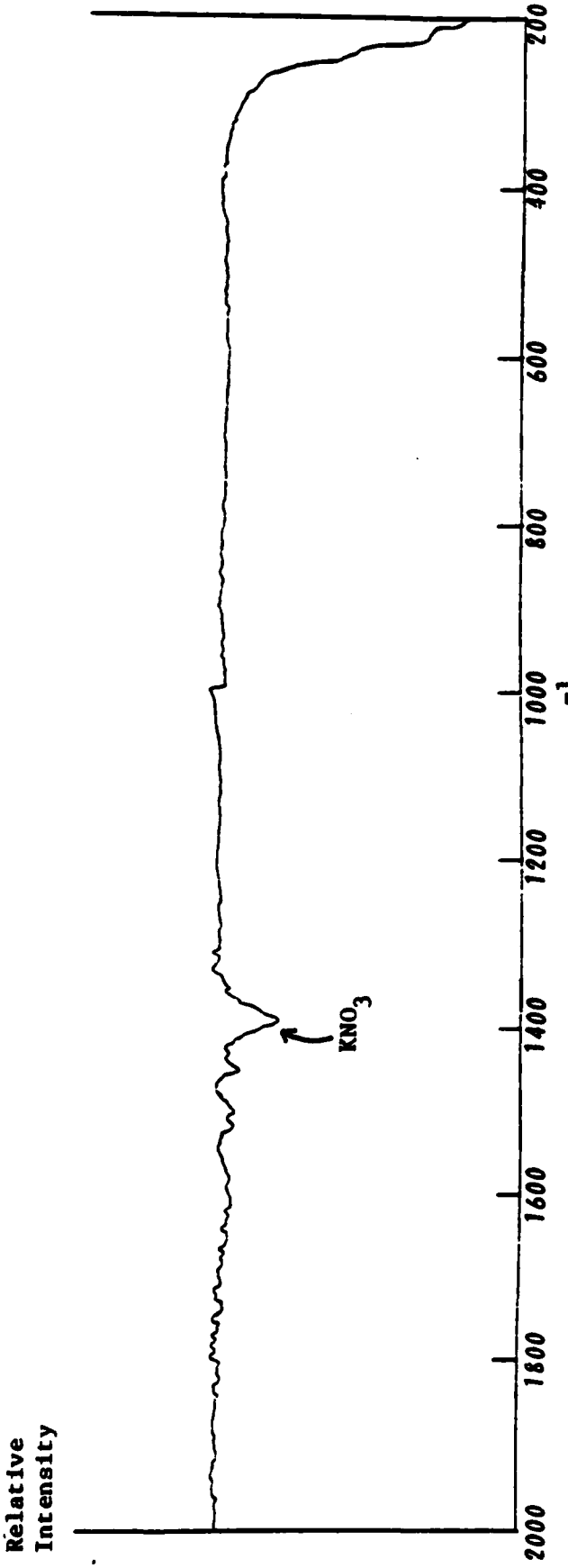

Figure 7. IR spectrum of blank KBr matrix.

pellet might be transparent enough, but there may not be enough graphite for any measurable level of interaction to occur.

This problem of finding a working mixture of KBr and graphite leads to a more serious objection. It is not clear that using IR spectroscopy is a valid method for determining the nature of species that may or may not exist as intercalants in a graphite lattice. The question remains as to whether the effective transmission of IR radiation through a pellet is due to the light passing through the graphite particles or to the light passing through the dilute pellets along paths where the graphite is absent. A piece of 10 micron graphite foil was placed in the IR beam and registered 0% transmittance throughout the IR range employed in these experiments (2000 - 200 cm^{-1}).

The paper[6] that claims evidence of CF and CF_2 bonding from IR spectra of graphite powders intercalated to stage I with SbF_5 attributes one of the peaks of their spectra to SbF_6^- ions. It is not clear that this association between the IR peaks observed and the above species is valid. As stated earlier, there is some question as to the ability of IR spectroscopy to give evidence of chemical species that may or may not exist within an intercalated graphite lattice.

Even if the problems of low transmission of IR radiation through graphite are ignored, there are still objections to the conclusions drawn in the aforementioned paper.

The peaks that are attributed to CF and CF_2 vibrations have values that are close to those for the two carbon-fluorine compounds. However, these values are for vibrational modes of the species when they exist in inert gas matrices.[7,8] It is not necessarily correct to assume that the vibrational modes of CF or CF_2 bonds will be the same in the two situations. In one case, the molecule is relatively free from interactions as it is suspended in an inert gas matrix. In the other, the fluorine or fluorines are bound to a carbon atom which is itself involved in a graphite lattice.

Following this same reasoning, those conclusions which assigned IR peaks to SbF_6^- ions must be re-evaluated. Once again, even if we ignore the suggested limitations of IR spectroscopy in these inquiries, we must question the veracity of linkages between vibrational modes of SbF_6^- as a free radical and peaks in an IR spectrum of graphite. Once again, there is no reason to assume that the modes of SbF_6^- will not change when it is locked in a graphite lattice. There is more reason to believe that the peak attributed to SbF_6^- should actually be linked with the vibrations of SbF_3.

SbF_3 has IR resonances at 654 cm^{-1} and 624 cm^{-1};[9] SbF_6^- has one at 669 cm^{-1}.[10] To the accuracy of IR spectroscopy, a peak in this region could be mistakenly attributed to either species. Small clear crystals were found growing in the ampoule with the stage I powder. A KBr matrix pellet was prepared from these crystals and a very strong peak was found centered about 660 cm^{-1}. (See Figure 8) Many of the X-ray diffraction spectra of SbF_5-intercalated powders show strong evidence of SbF_3 crystals. Some of these spectra were of powders that were allowed to de-intercalate.

An attempt was made to see if the CF or CF_2 bonds would result after a pellet was allowed to react with air over a period of time. A pellet was prepared using the stage II powder. The initial spectrum showed evidence of the peak traditionally assigned to SbF_6^- vibrations (Figure 9). IR spectra were run over a period of a week, more than enough time for the sample to react with air. During this period, the spectrum did not vary significantly in any way. The small peak around 660 cm^{-1} remained in the entire series; in fact, if anything, it became stronger. If this peak was actually due to SbF_6^-, it should have disappeared during this period after the powder had time to de-intercalate. As it did not disappear and noting that SbF_3 tends to be a product

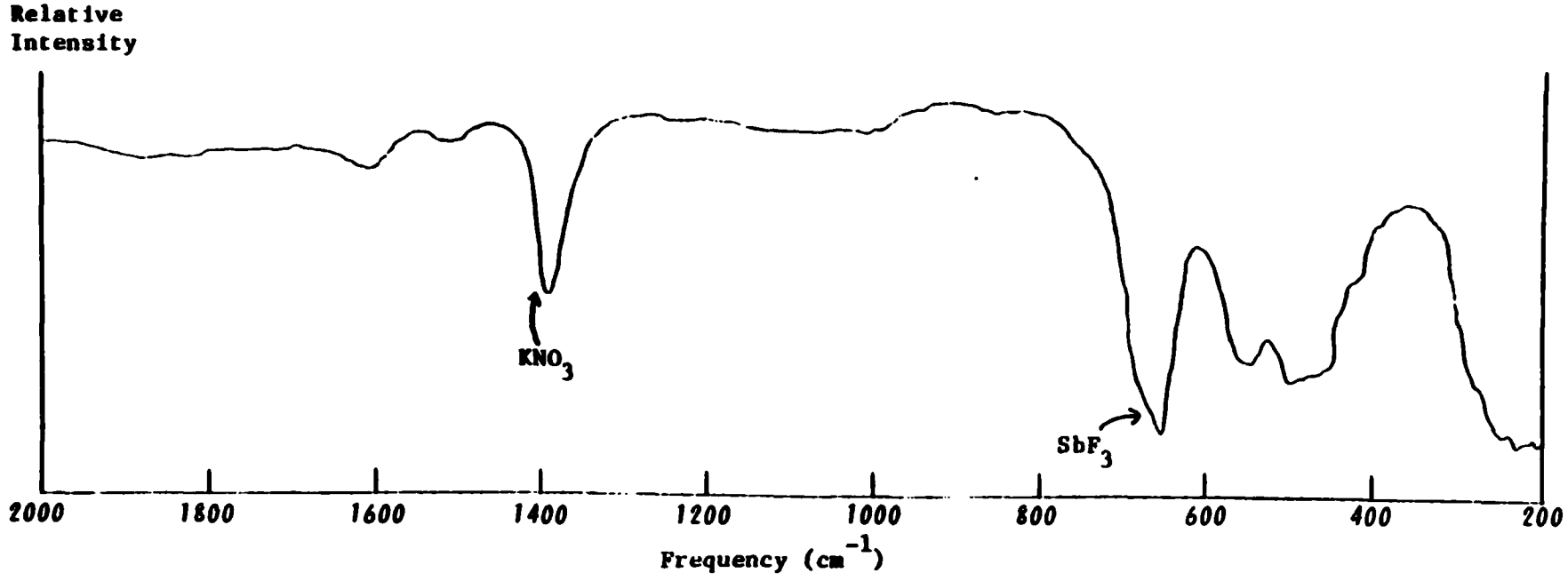

Figure 8. IR spectrum of KBr matrix prepared with clear crystals from stage I SbF_5 graphite powder.

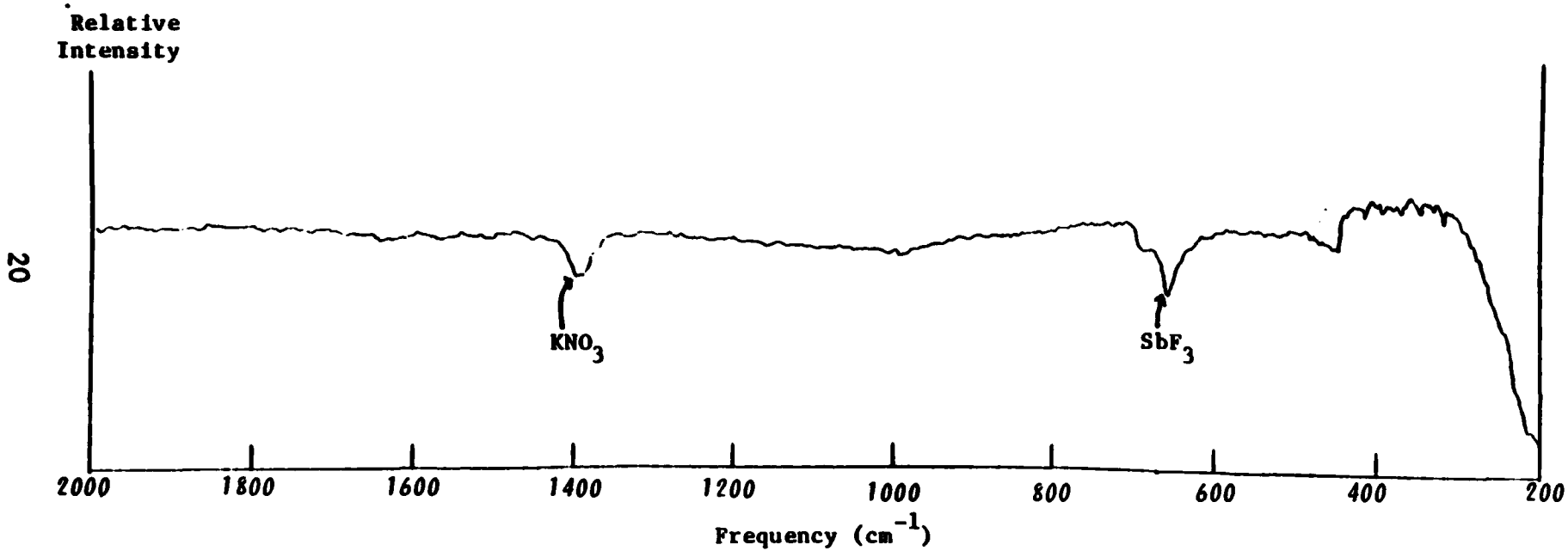

Figure 9. IR spectrum of KBr matrix prepared with stage II SbF_5 graphite powder.

of the de-intercalation process, it is more reasonable to assign that peak to SbF_3 and not SbF_6^-.

G. Conclusions

Due to all the above mentioned objections and results, a number of conclusions can be made. First and foremost is the suggestion that IR spectroscopy is an invalid approach at analyzing the intercalant species of a graphite compound. At best, it may give evidence of molecules that result from processes associated with the graphite compounds and which exist either free of or on the surface of the graphite crystals. With this in mind, it is reasonable to conclude that those IR results previously attributed to SbF_6^- ions are actually due to SbF_3, which is present either as a product of the intercalation reaction, a product of the de-intercalation process, or both. The evidence of CF and CF_2 bonding in intercalated powders found in earlier research must be assumed to show such bonding only external to the graphite lattice. Any direct conclusions on the nature of species inside a graphite lattice should not be based on IR spectroscopy results.

III. Swaging Composite Wires of Copper and Intercalated Graphite

A. Introduction

Attempts have been made at finding applications for the enhanced electrical properties that graphite gains upon intercalation. One of these has been in the production of swaged composite wires consisting of an intercalated graphite core encased in a metal sheath. This most recent work dealt with SbF_5 as the intercalant and copper as the sheath material. The idea is to end up with a wire which conducts electricity better than conventional conductors, but is lighter and uses less expensive material.

It should be stated at the onset that this effort did not yield the desired results for reasons that will be explained. What follows is a description of those procedures that were tried. Hopefully, this will be useful as a reference for any future work into this problem.

B. Procedures

The single largest problem in the preparation of swaged composite wires is the occurrence of cracks and fissures in the copper sheath which develop during the swaging process.

This exposes the air-sensitive SbF_5 intercalated graphite, producing a useless wire. Unfortunately, those wires which were successfully swaged to a sufficiently small size showed resistivities, when measured with a Kelvin bridge, higher than that for a pure copper wire.

1. Ampoule Geometry

The first task was to find a metal geometry which at least tended to minimize the cracking problem during swaging. This consisted mainly of varying the ID to OD ratio in the copper ampoule. A smaller ratio meant less frequent splitting, but also meant that less graphite was being used in the composite. After many attempts, the configuration shown in Figure 10 was chosen. The ampoules made during this early work were machined out of stock copper rod. Once the geometry was decided upon, only OFHC copper rod was employed in order to maximize the conductivity of the composite.

In the initial work done in investigating the geometry issue, the ampoules were found to swage better if they were filled loosely with graphite rather than packing them full using a hammer and plunger. This method, called tap filling, involved letting the graphite settle by tapping the ampoule gently on the table as it is filled. Although less graphite

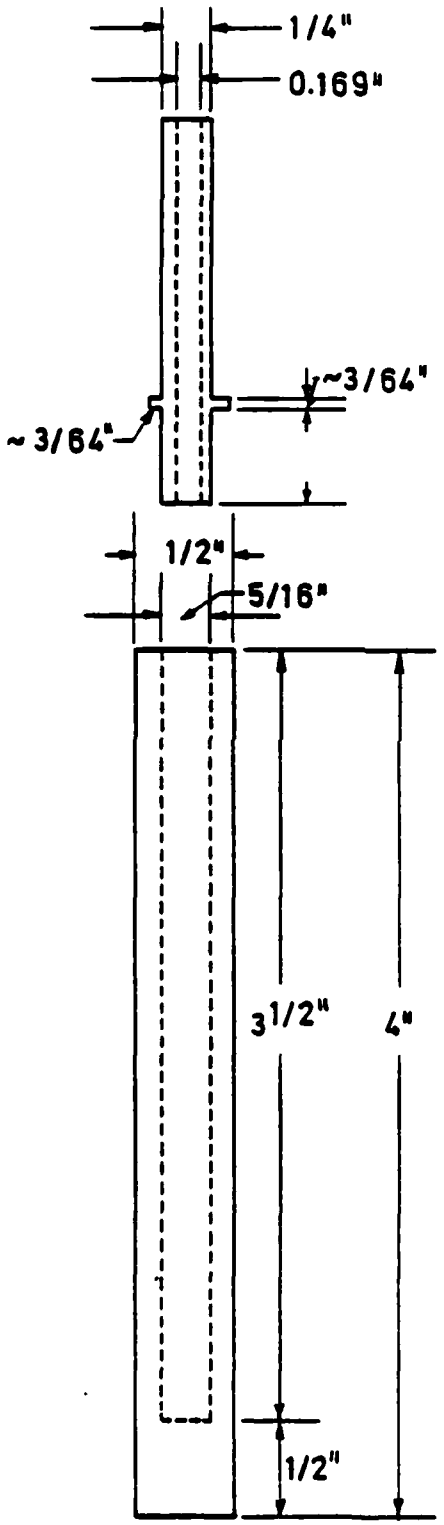

Figure 10. Copper ampoule used for preparation of swaged wires.

was used, somewhat better success was achieved for the swaging process.

2. Filling Techniques

Numerous different methods were tried in the preparation of the ampoules for the swaging process. Some of these involved filling the ampoule with pristine graphite powder and then intercalating with SbF_5. Others used pre-intercalated powders as the filler.

The first series of experiments attempted to have the intercalation proceed after the ampoules were filled with pristine graphite (Superior #2001). Initially, the caps were arc-welded to the ampoules after the ampoules were already filled with graphite. This proved difficult as the graphite would tend to interfere with the welding process, often leaving the seal with leaks. To alleviate this problem, the caps were welded first and filling was done later. This made it possible to leak check the ampoules before filling them with graphite.

After tap filling an ampoule (with typically about 2.5 gm of graphite), a small ball of fine copper wire is placed on top followed by some pyrex glass wool. These last two are used to prevent the graphite powder from being sucked

into the vacuum line, but either or both are optional if caution is observed while evacuation is performed. The ampoule is connected to the apparatus shown in Figure 11. While being pumped on overnight, the ampoule is heated to about 150°C to remove any water in the system.

After the drying out of the graphite is completed, the ampoule is sealed off and attached to a graduated cylinder as in Figure 12. In a glove box, 1-2 ml of SbF_5 is added to the cylinder side, which is then capped with a stop-cock ground glass joint connector for removal from the glove box back to the vacuum line.

Now on the vacuum line, the cylinder side is evacuated of the glove box atmosphere and the SbF_5 is pumped on to remove unwanted absorbed gases. The cylinder and ampoule arrangement is sealed off from the vacuum line, the break-seal is broken, and the set-up is placed in an oven ($\sim$140°C). After baking for up to 600 hours is some cases, the ampoules were crimp-sealed just below the Swagelok connection. They were then swaged and when possible measured for resistivity.

A second method involved half-filling the ampoules with dried out graphite in a glove box. SbF_5 was then pipetted directly into the ampoules, followed by enough graphite to tap fill. The ampoules were sealed with a Swagelok plug,

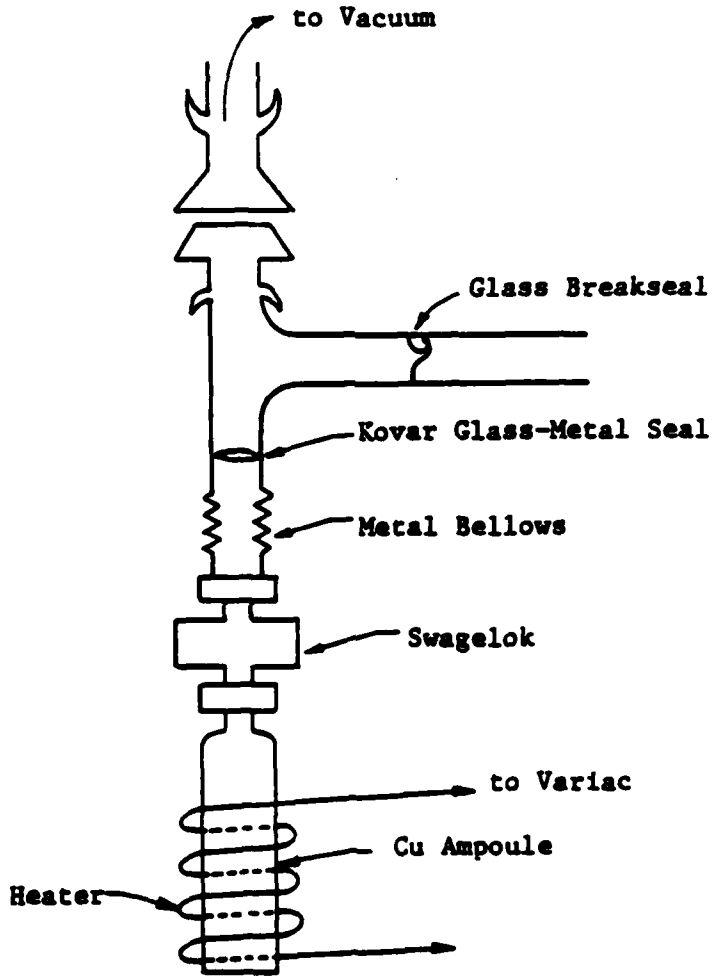

Figure 11. Apparatus for drying out graphite powder for swaged wires.

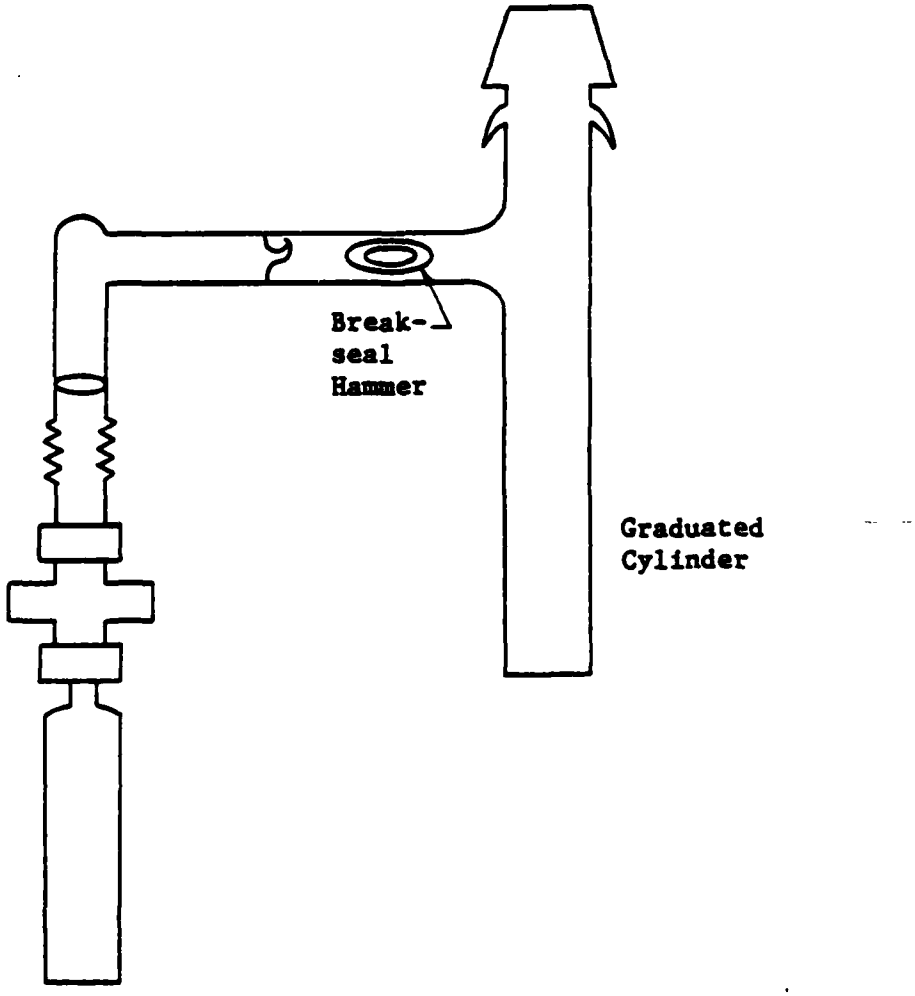

Figure 12. Apparatus for adding SbF_5 to graphite for swaged wires.

removed from the glove box, and baked at 150°C for about 45 hours. Different amounts of SbF_5 and graphite were used.

The third method utilized pre-intercalated SbF_5 graphite powders of various stage as the filling material. The ampoules were tap filled in a glove box and crimp-sealed for immediate swaging.

Other procedures involved attempts at reconstructing earlier work done by Jim Gan.[11] Ampoules of OFHC copper were machined as shown in Figure 13. Three different methods were employed.

A. After filling an ampoule half way with dried pristine graphite (Superior #2135) in an inert atmosphere glove box, enough SbF_5 ($\sim$.3 ml) was pipetted in to yield a 50%-50% mixture by mass of graphite and SbF_5. The rest of the graphite powder was added and then the ampoule was sealed. Sealing was done by adding some copper powder and closing the opening with a plug of solid Pb/Sn solder. The seal was secured by melting the solder in place with a hot soldering iron.

B. After filling an ampoule half way with Graphimet 50-50, 5 drops of SbF_5 ($\sim$.02 ml) were added before the rest of the graphite based mixture was included. The ampoule was sealed as in A.

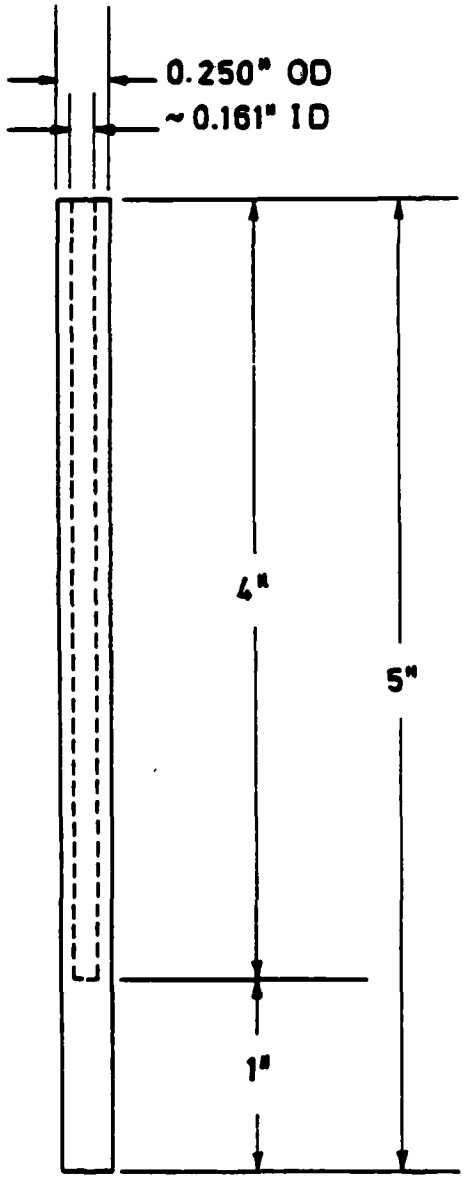

Figure 13. Thin copper ampoules used for preparation of swaged wires.

C. After filling an ampoule half way with Graphimet 50-50, $\sim$.15 ml of SbF_5 was added, followed by the rest of the Graphimet. The ampoule was sealed as in A.

The ampoules were removed from the glove box and immediately swaged. Besides the usual cracking problems, the plugs slowly worked themselves out further with each reduction in the swaging process.

C. Results

The problems of cracking and splitting of the wires during swaging remained the largest problem. Less than 40% of the wires were undamaged after swaging from .5" OD to .125" OD. Annealing the Cu ampoules at 850 C for 1 hour before filling did not reduce the cracking problems.

Although most of the wires showed low resistivities, averaging about 1.9 $\mu\Omega$-cm, this could very well be due almost entirely to the copper sheath conductivity. Chemical analysis (performed by A. Varma) of wires of .125" OD showed that 98-99.5% of the wire mass is copper. There is a graphite core after swaging as can be seen by dissolving away the sheath in HCl or HNO_3. The procedures for the analysis of Sb content in the wires were very unreliable.

IV. Pressing Pills

A. Introduction

Much work has been done in attempting to fabricate wires which successfully utilize the reported high conductivities of intercalated graphite. This usually involves the swaging or drawing into composite wires of metal ampoules (e.g. Cu, Al, Pb) filled with an intercalated graphite powder. During these processes, the graphite is subjected to mechanical and thermal conditions which may affect the nature of the intercalation.

The conductivity of intercalated graphite is highly dependent on the type of intercalant and on the stage of the intercalation. Besides possible affects on the intercalation itself, the stresses of swaging may enhance the overall conductivity in other ways. It has been seen[2,11] that during the swaging process the particles of graphite tend to arrange themselves with their c-axes pointing radially. Since the conductivity of graphite in the a-axis direction is larger than in the c-axis direction, this orientation of the crystals enhances the overall conductivity of a composite wire.

It is also possible that the swaging process helps shore up crystal boundaries and increase crystal contact areas; thus, decreasing the number and size of recombination sites which limit the conductivity. In order to study some of these affects, experiments were performed pressing into pills powders of pristine and intercalated graphites under various conditions.

B. Experimental Procedures

1. Pill Geometry Considerations

In earlier work dealing with pressing graphite, square pills (5 x 5 mm) were prepared in order to imitate the shape and size of the HOPG samples that are generally used in other experiments. There were problems, however, with this geometry.

First of all, presses that would yield pills of those desired dimensions consistently were difficult to make. They failed to retain their geometry under the stresses of the high pressures used in the preparation of the pills. The other problem involved the fragility of square pills made from powders. It was difficult to get a sturdy pill whose corners did not tend to break off.

2. Press Design

For these reasons, the press was designed to make round pills. The press itself was easier to assemble due to its fewer parts and the pills tended to hold up better under handling. The first press design (Figure 14) turned out to be ineffective. The powders leaked out the bottom when pressure was applied. The improved press (Figure 15) proved to be very effective at pill production.

3. Recalibration of the Resistivity Measuring Apparatus

The change from square to round pills necessitated a recalibration of the contactless R.F. induction apparatus used for the resistivity measurements of the pills. This was accomplished with a number of OFHC copper pills machined to the desired size (i.e. 5 mm diameter). A calibration constant K of .131 was found as compared to .122 for the square samples. Qualitatively, this makes sense as a larger K value is expected for a geometry of smaller area. (For an indepth discussion of this measurement technique, see T.C. Wu's PhD dissertation, pp.24-43.)

Since the induction apparatus has a tendency to drift over time, it was important to check whether the ΔV values were independent of the initial and final voltages measured.

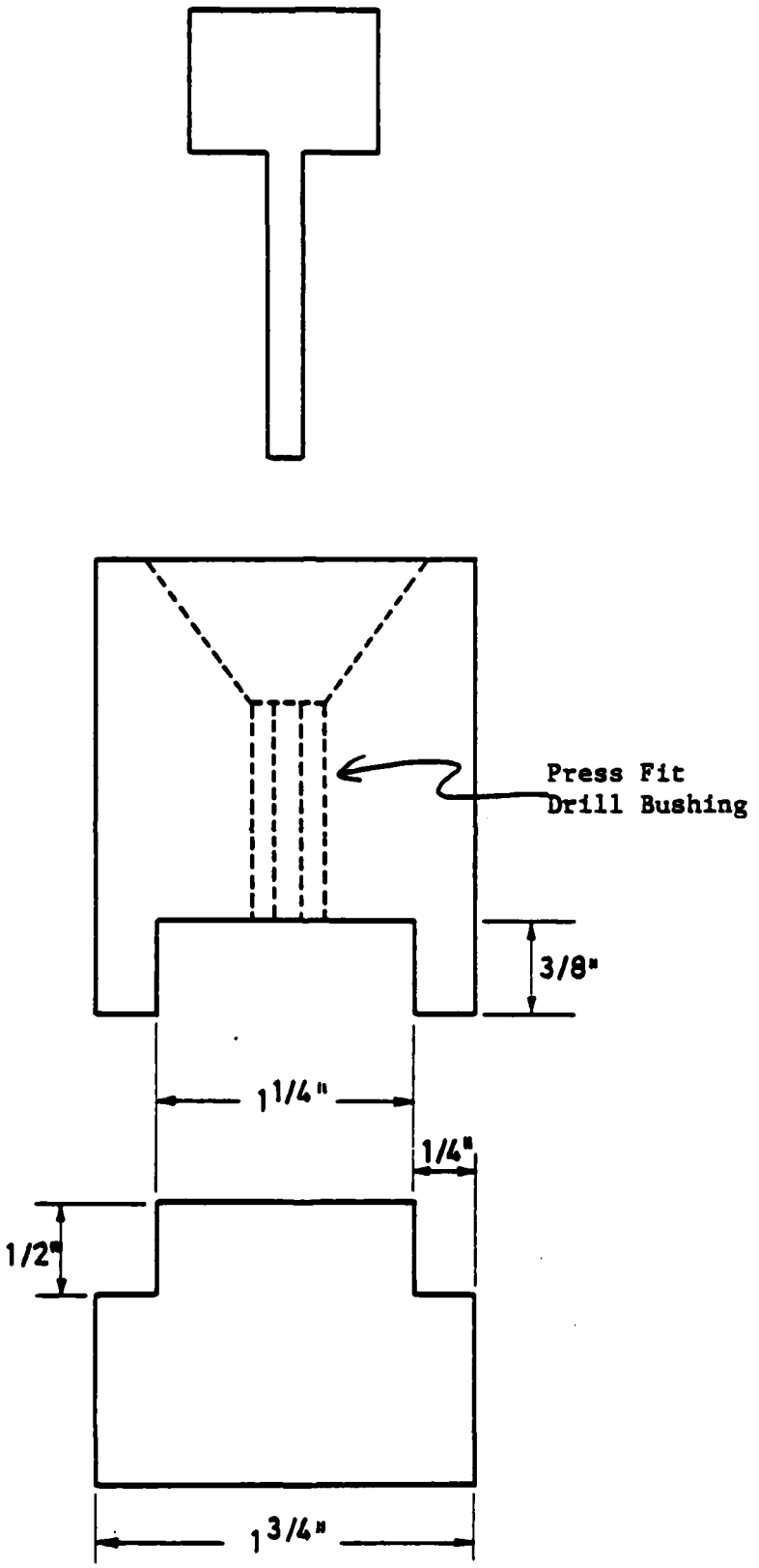

Figure 14. Press design A for preparing graphite powder compacts.

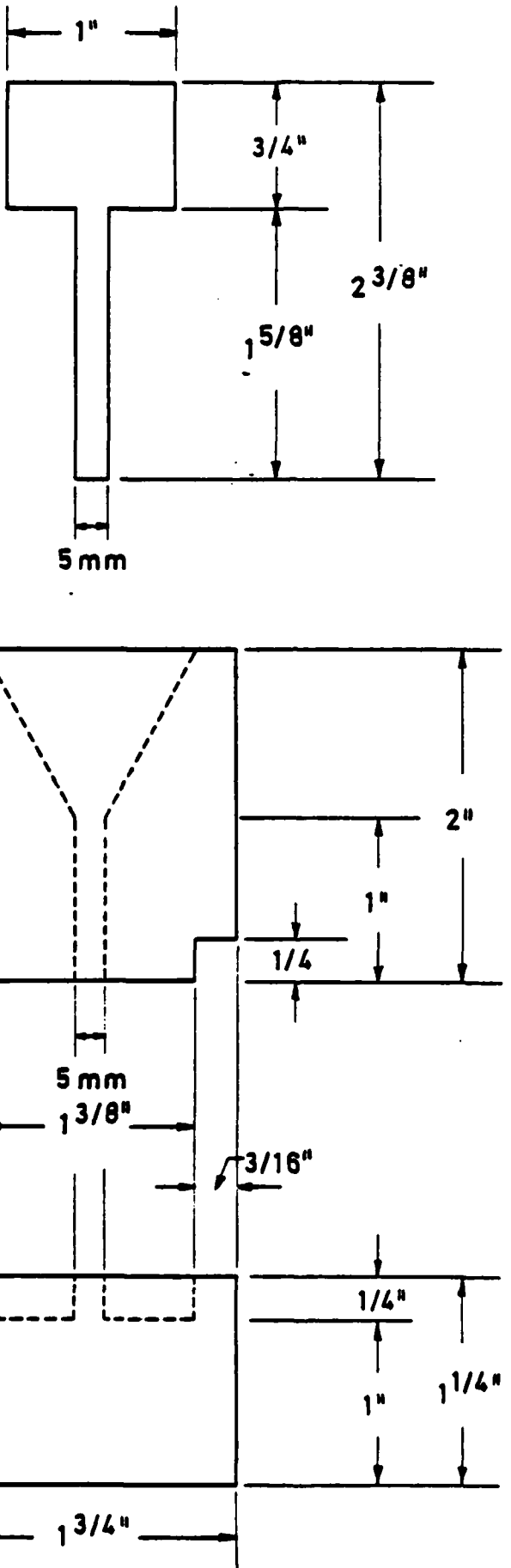

Figure 15. Press design B for preparing graphite powder compacts.

By adjusting the fine tuning, it was possible to measure ΔV for various ranges above and below the zero value. It was found that ΔV was indeed independent of the initial and final voltages over a large enough range to insure the reproducibility and compatibility of results from day to day.

4. Pill Storage

Many of the pills were prepared from intercalated graphite powders that are air-sensitive (e.g. SbF_5). It was necessary to devise a holder for these pills that allowed for the contactless conductivity measurements and also insured the stability of the pills themselves. A drawing of the design used is shown in Figure 16.

5. Pill Production Techniques

Although pressed pills were prepared in many different ways, these procedures usually only varied slightly. A description of the procedure used for preparing pills at room temperature of air-sensitive powders is given here. Alternate procedures will be explained as the individual experiments are explained.

In an inert atmosphere (e.g. an argon filled glove box), a small amount of graphite powder (already intercalated

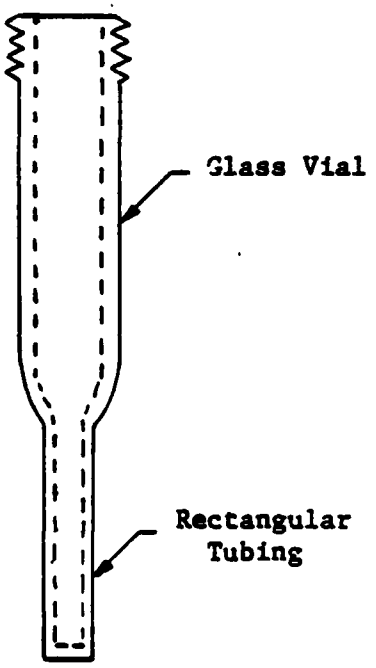

Figure 16. Glass sample holder for compacts made from air-sensitive intercalated powders.

and characterized) is placed into the press with the plunger removed. The plunger is then inserted and the desired pressure is applied (on a Buehler press) for a known period of time. The pill is removed by forcing it out with the plunger. It is then weighed and its thickness measured with a micrometer.

After placing the pill is the test tube (Figure 16), the cap, which has had silicon stopcock grease applied to insure an air-tight seal, is firmly screwed on. The sample can now be removed from the glove box for measurement of its resistivity on the contactless induction apparatus.

The procedure for preparation of pills from air-stable graphites is similar, but without the requirements of an inert atmosphere or storage in an air-tight sample holder.

The initial work involved pressing pills at room temperature at various pressures for various lengths of time using different graphites in both the pristine state and intercalated with SbF_5 to different stages. These included Superior graphites #2001, #2135, and #4735.

The #2001 powder is much coarser than the other two. Over 50% of the #2001 passes through a 200 mesh in a typical screen analysis.[12] In a similar analysis of the other two graphites, fully 99% of the powder passes the 325 mesh

screen.[13,14] Samples of #2001 were mixed with SbF_5 to yield compounds of stage I, II, III, and IV. The other graphites were also intercalated with SbF_5 in a 50%-50% mass ratio, which gives a stage II compound.

6. Pulsed Pressure

During one of the pills' preparation, the valve on the Buehler press was not sufficiently tight. This resulted in a constantly dropping pressure. To counteract this, the pressure was periodically increased to the desired level. The result was a pill prepared using what is here termed pulsed pressure. It is possible that this action more closely simulates the stresses administered to the graphite during the swaging process. A series of pills were made using this pulsed pressure.

In general, when the variable being tested was pressure, the time of application was 30 seconds. Pressures ranged from press readings of 1 Klb to 9 Klb. (For conversion from press reading to pressure on powder see Table 2.) When time was the variable, ranging from 15 seconds to 32 minutes, the force was fixed at 4 Klb.

Table 2. Conversion table from press force to pressure on 5 mm diameter compacts.

Press Force	Pressure	
1 Klb	33000 PSI	2.3 Kbar
2	66000	4.5
3	99000	6.8
4	131000	9.1
5	164000	11.3
6	197000	13.6
7	230000	15.9
8	263000	18.1
9	296000	20.4

7. Annealing Pills

A set of experiments were run to see what affect annealing might have on the conductivity of prepared pills. Pills were made from a stage II SbF_5 compound and, after being weighed and measured, were placed in holders similar to the one shown in Figure 17. A small amount ($\sim$1 ml) of SbF_5 was pipetted into the test tube side of the pyrex holder. After capping with a stop-cock connector, the set-up was removed from the glove box and attached to a vacuum line.

The system was then opened to a liquid nitrogen cold trap for about 3 minutes. At this point, the line was opened to the forepump to help remove the argon from the glove box as well as to boil off any non-condensable gases from the SbF_5.

After the SbF_5 ceased to boil, the stop-cock was closed and the set-up was given time to equilibrate. After about 5 minutes, the sample was sealed off from the apparatus in the hope that what remained was a pill made from a stage II SbF_5 graphite compound in an atmosphere of SbF_5 vapor. The samples were then baked at various temperatures (200, 300, and 400°C) for 24 hours.

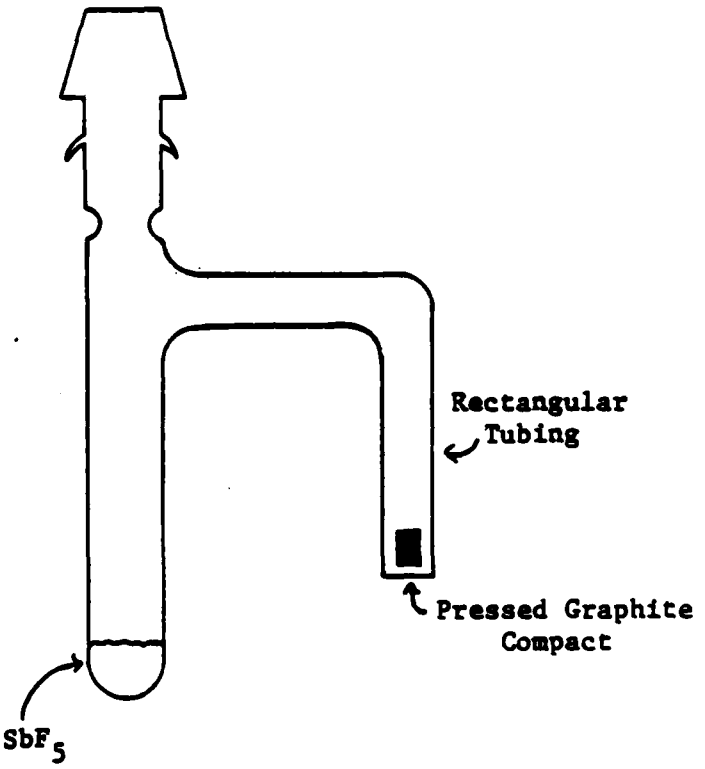

Figure 17. Glass sample holder for annealing graphite powder compacts in SbF_5 vapor.

A similar set of experiments were run using pills prepared with an air stable graphite compound, stage III $CuCl_2$. These samples were pressed, weighed, and measured before being placed on a vacuum line. The sample tubes were evacuated (pumped on for 3 minutes) and sealed before being placed in ovens at 200 and 300°C for about 24 hours.

8. High Temperature Pressing

The first attempt at heating the powder as it was being pressed was disasterous. Probably due to a combination of the heat, pressure, and length of time both were administered, the graphite flowed and slipped into the gaps in the press causing the entire assembly to be fused together. In order to save the press, the pill was sacrificed.

In an effort to alleviate this sticking problem, a press set-up was used with the middle piece made entirely of teflon. This was unsuccessful as the pressure used was too great for the teflon to withstand. The answer to these problems was to use the all steel press with small teflon spacers to keep the graphite in place.

These teflon spacers were prepared by pressing teflon pipe tape at 8 Klb for a second or two. Typically, each one was about .2-.3 mm thick and weighed about .01 gm.

This solution was not without its limitations either as it was found that the teflon itself began to flow and cause fusing problems at press readings above 2 Klb.

With this teflon spacer method, pills were prepared from pristine graphite #2135 as well as the stage II SbF_5 graphite #2001 and stage III $CuCl_2$ graphite KS75B (75 micron particle size). The temperature at which these pills were heated was 175°C. The times ranged from 20 minutes (from the time the heater was turned on to when the pressure was relieved) to 120 minutes and the force was kept at 2 Klb.

X-ray diffraction spectra were taken to compare the $CuCl_2$ intercalated graphite before and after pressing for 2 hours at 175°C.

C. Results and Discussion

Tables 3 and 4 and Graphs 1-3 relate three variables: the pressing force used in pill production, the density of the pill compact, and its resistivity as measured with the contactless device. These are for compacts made from various pristine and intercalated graphite powders.

There seems to be some correlation between the compact resistivity and the pressing force used in its preparation, especially at the lower pressure levels (Table 3). In 5 of

COMPACT MATERIAL

Pressing Force	Pristine #2135	Pristine #2001	Stage IV SbF_5 #2001	Stage III SbF_5 #2001	Stage II SbF_5 #2001	Stage II SbF_5 #2001 Pulsed Pressure	Stage III $CuCl_2$ KS75B
1 Klb	———	———	125±3	———	132±4	120±4	———
2	1020±130	———	115±3	80±3	111±7	106±3	700±100
3	920±120	380±20	106±3	88±5	104±3	99±3	———
4	850±90	320±20	109±5	89±3	101±4	107±3	560±70
5	1070±150	340±20	102±2	85±3	98±6	98±3	410±50
6	1040±130	370±20	111±4	87±2	96±3	100±3	420±30
7	———	340±20	101±3	82±2	———	———	———
8	———	300±20	———	———	———	———	———
9	———	320±20	———	———	———	———	———
Average Resistivities	940±130	340±30	110±8	86±4	103±10	105±8	430±60

Table 3. Compact Resistivity vs. Pressing Force.

All samples prepared by pressing at room temperature for 1/2 minute under constant force, except for compact made with pulsed pressure. All resistivities are in μΩ-cm.

the seven materials and/or techniques used, there is a decrease in resistivity with increasing pressure for at least the lowest three pressure values. In fact, the results for the compacts made from the stage II SbF_5 #2001 show this trend throughout the force range employed.

It may be that when the pressing force reaches 3-5 Klb, the compacts have already reached their limit as far as mechanically pressing the powders can reduce their resistivities. Noting that the stage III SbF_5 #2001 has the lowest resistivities and thus the most metallic-like properties, it may reach its pressing saturation point at a lower pressure than the others due to its greater malleability.

It is impossible to make similar conclusions in regards to any correlation between compact density and pressing force from the results in Table 4. Absolutely no trends or patterns are obvious. This is odd, in view of the clear pattern linking resistivity and pressure at the lower levels.

Fig. 18 shows the relationship between compact resistivity and density for two different sized pristine graphite powders, #2001 and #2135. Together they show a possible trend towards lowered resistivity with higher density as is expected.

COMPACT MATERIAL

Pressing Force	Pristine #2135	Pristine #2001	Stage IV SbF_5 #2001	Stage III SbF_5 #2001	Stage II SbF_5 #2001	Stage II SbF_5 #2001 Pulsed Pressure	Stage III $CuCl_2$ KS75B
1 Klb	———	———	2.33±.03	———	2.52±.03	2.61±.04	———
2	2.03±.02	———	2.35±.03	2.48±.05	2.55±.07	2.63±.03	2.17±.03
3	1.97±.02	2.17±.02	2.10±.03	———	2.58±.03	2.57±.03	———
4	2.04±.03	2.12±.02	2.33±.02	2.36±.05	2.54±.05	2.56±.03	2.32±.03
5	2.02±.02	2.14±.03	2.36±.03	2.38±.05	2.63±.09	2.67±.03	2.33±.05
6	2.06±.02	2.17±.02	2.36±.04	2.42±.04	2.50±.04	2.49±.04	2.33±.03
7	———	2.16±.02	2.37±.04	2.83±.04	———	———	———
8	———	2.15±.03	———	———	———	———	———
9	———	2.16±.03	———	———	———	———	———
Average Densities	2.04±.04	2.15±.02	2.32±.09	2.43±.15	2.57±.09	2.59±.06	2.33±.04

Table 4. Compact Density vs. Pressing Force.

All samples prepared by pressing at room temperature for 1/2 minute under constant force, except for compacts made with pulsed pressure. All densities are in mg/mm^3.

Fig. 18 Resistivity vs. density for pristine graphites #2001 and 2135.

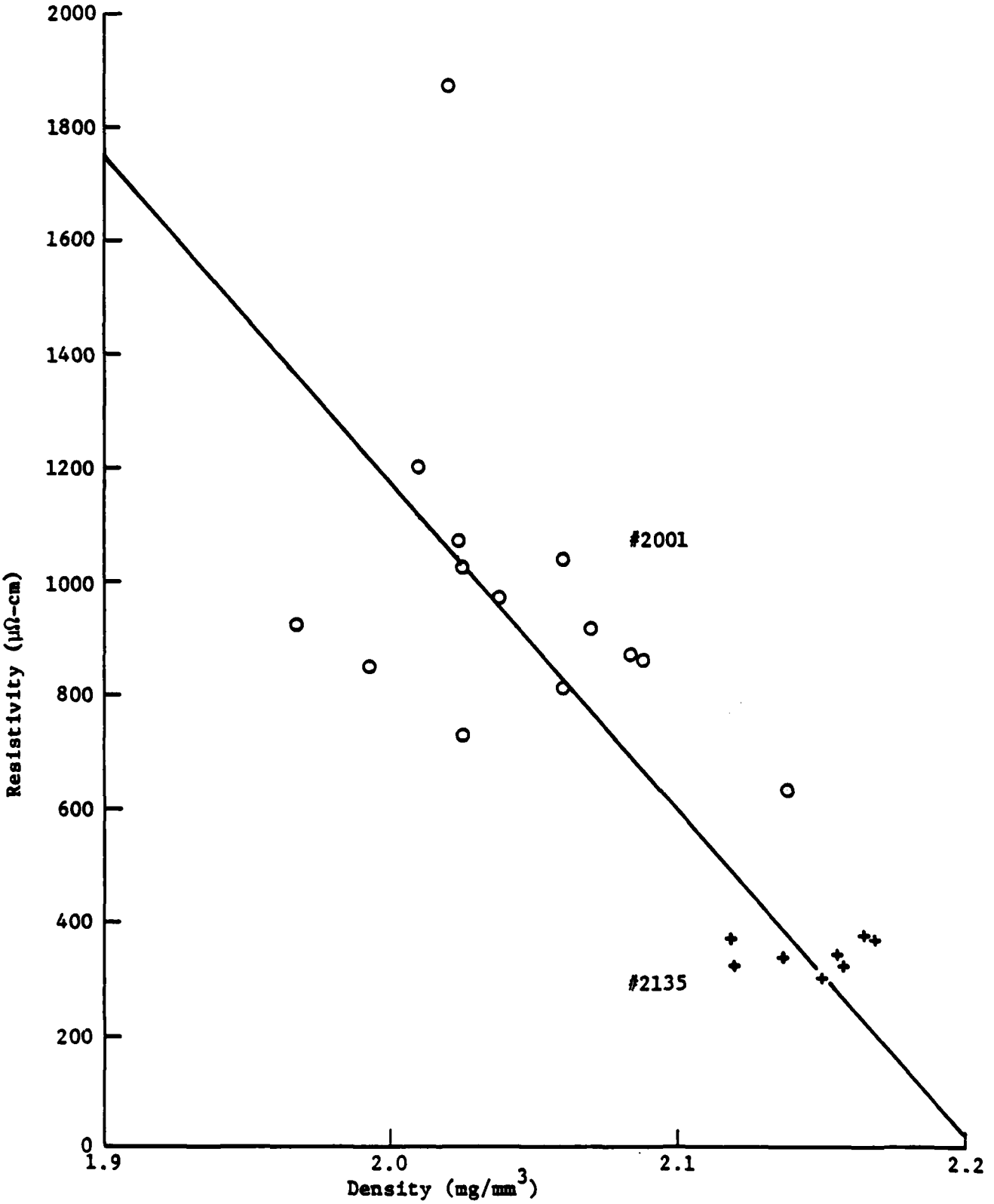

This tendency is also suggested in Fig. 19 where the same variables are related for compacts made from the stage III $CuCl_2$ KS75B. The large scatter in both of these cases makes assigning a line or a curve very difficult.

Fig. 20 plots resistivity and density for compacts prepared from SbF_5 intercalated graphite #2001 for stages I, II, III, and IV. Although lines can be drawn through three of the sets of points with some confidence, this is not the case for the stage II compacts.

The results from pressing compacts from stage II SbF_5 #2001 at room temperature and at 4 Klb for varying lengths of time are shown in Table 5. The lack of any clear trend at this force level seems to substantiate the notion of a pressure saturation level previously explained.

There are obvious indications for a dependence of resistivity and density based on the stage of intercalation (see Figs. 21 & 22). The density results are especially nice as they follow the calculated theoretical values.[15] The lower densities are expected since the compacts are made from randomly oriented powders and are not expected to be as dense as perfectly oriented ideal graphite crystals.

Fig. 19. Resistivity vs. density for stage III $CuCl_2$ intercalated graphite KS75B.

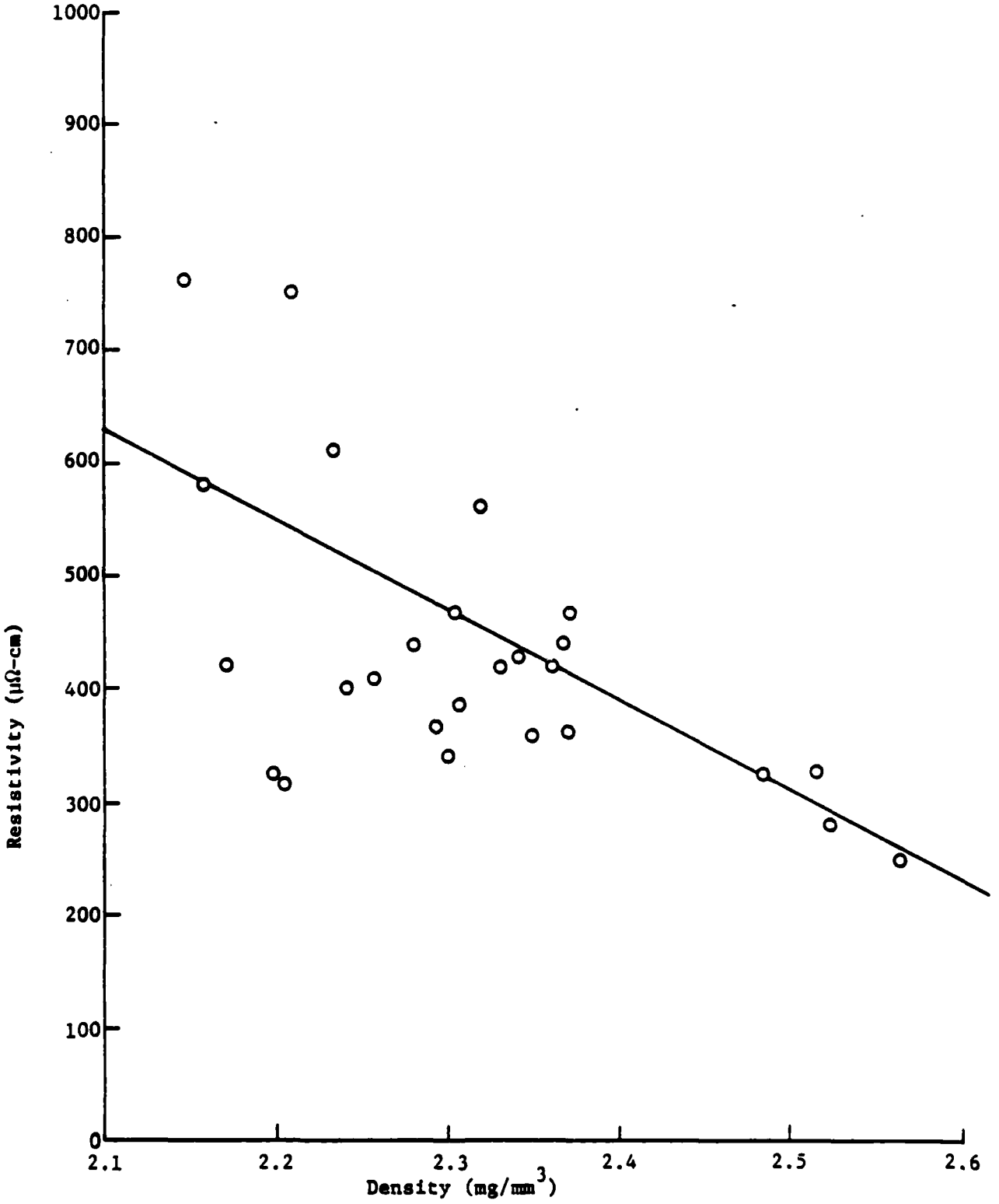

Fig. 20 Resistivity vs. density for SbF_5 intercalated graphite #2001 for stages I, II, III, and IV.

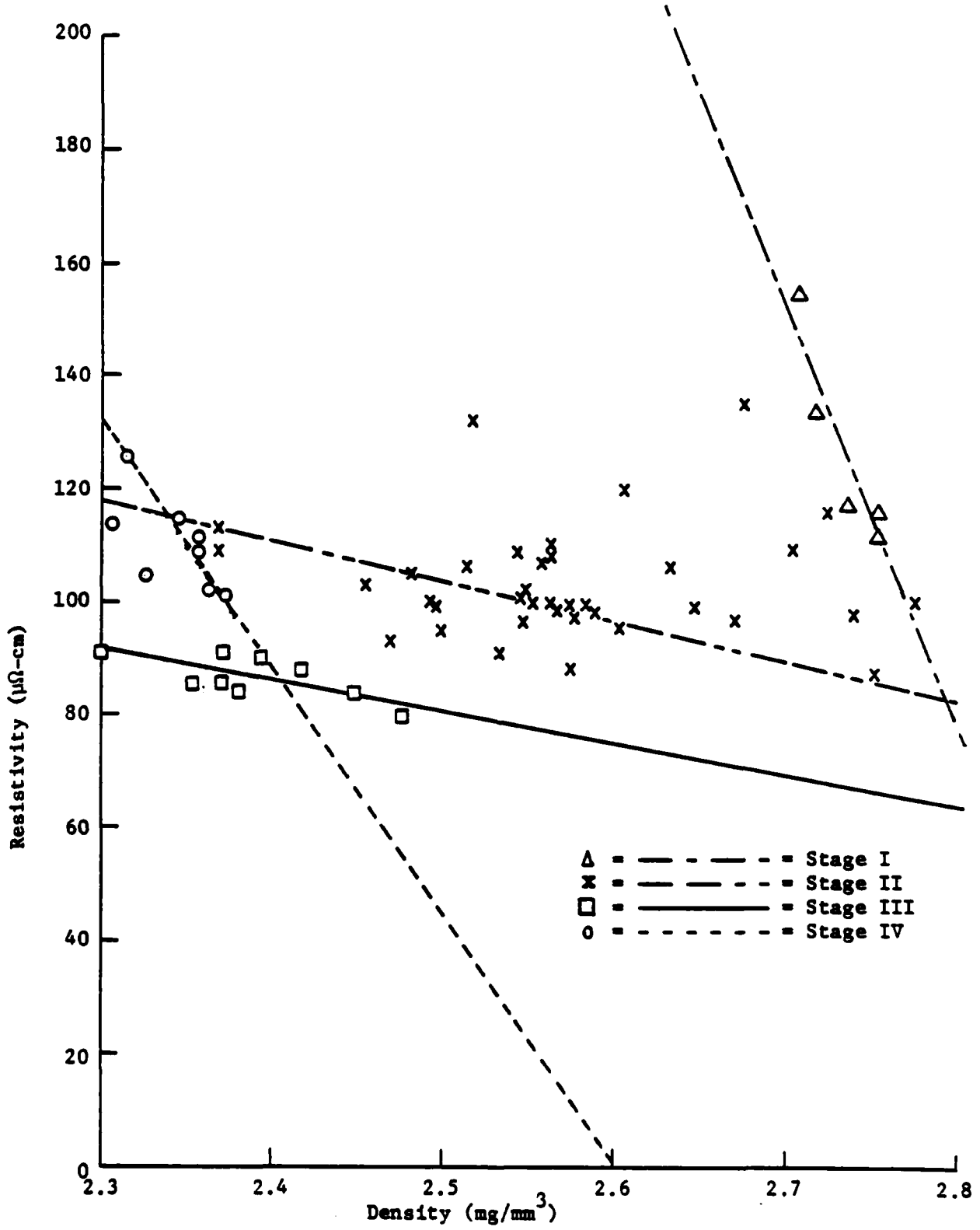

Table 5. Compact resistivity and density vs. time of applied pressure.

Compacts made from stage II SbF_5 #2001 at room temperature at 4 Klb.

Time (min)	Resistivity ($\mu\Omega$-cm)	Density (mg/mm^3)
.25	102±4	2.55±.04
.5	105±4	2.48±.04
1.0	93±3	2.47±.04
2.0	95±2	2.60±.03
4.0	99±3	2.56±.04
8.0	103±3	2.46±.03
16.0	109±3	2.50±.03
32.0	106±3	2.51±.03
Average Values	103±10	2.57±.09

Fig. 21 Resistivity vs. stage for SbF_5 intercalated graphite #2001.

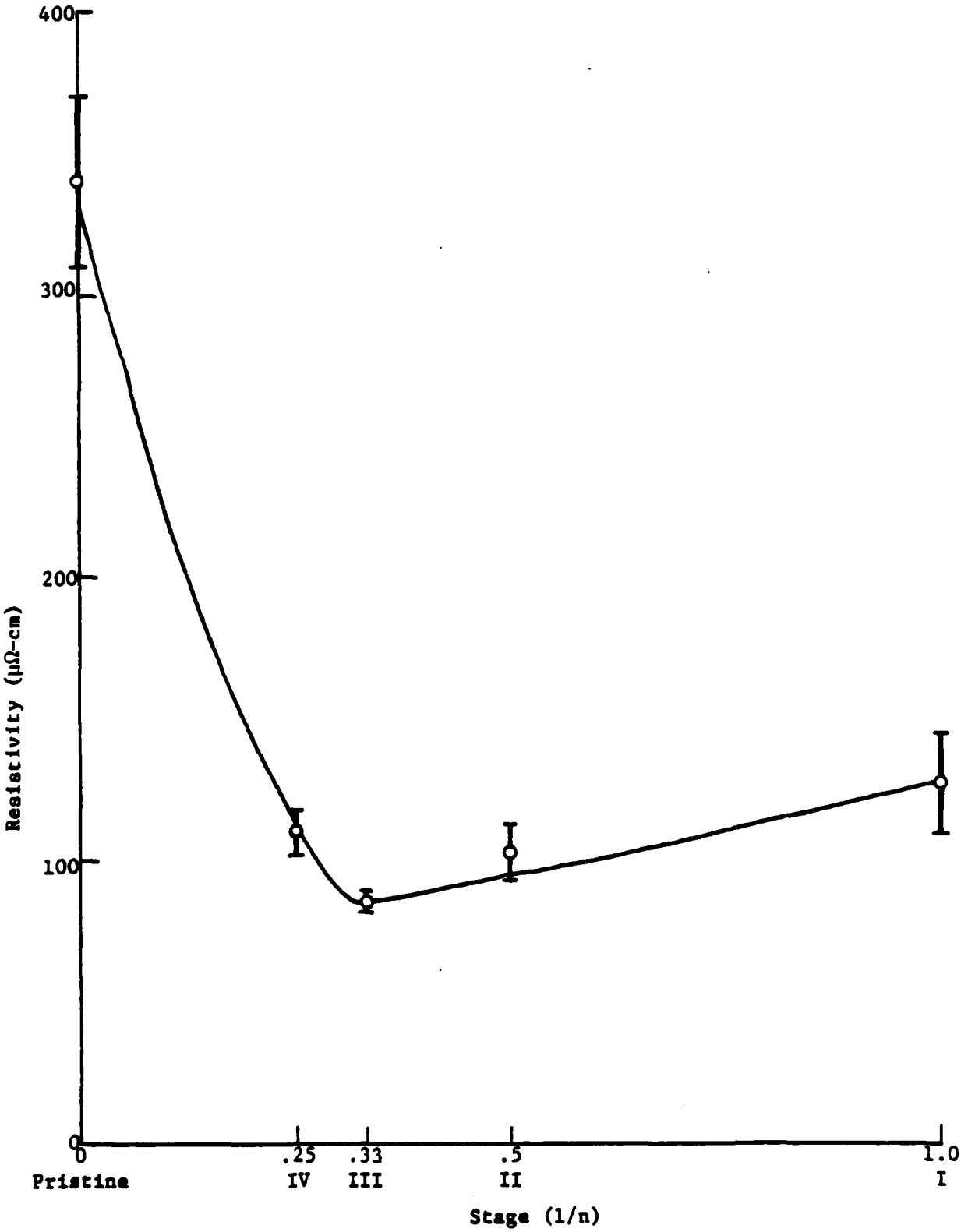

Fig. 22 Density vs. stage for SbF_5 intercalated graphite #2001.

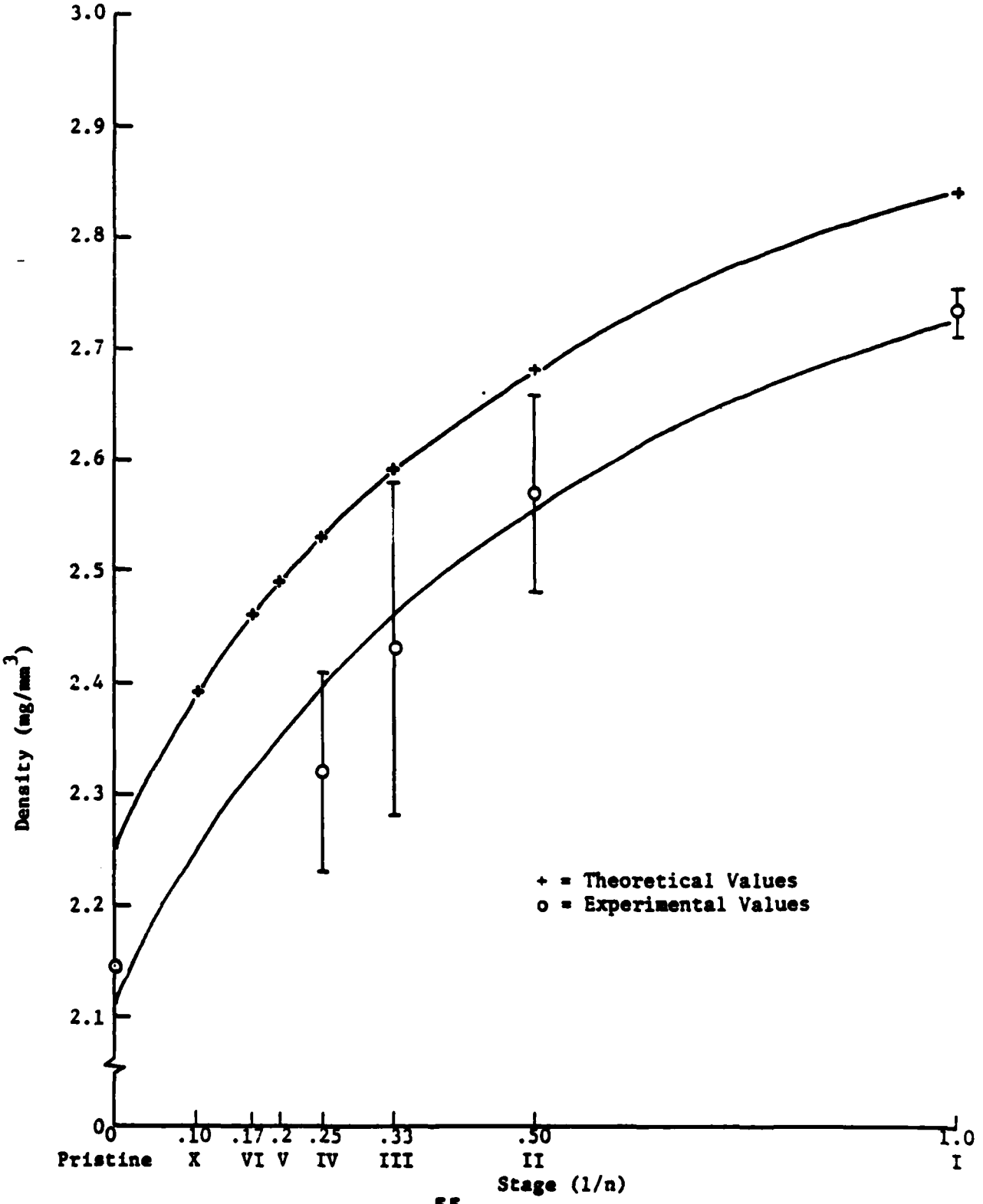

Comparisons of results between different powders is also possible (Fig. 23). It makes sense that the densities would be higher and the resistivities lower for the #2001 powder than for the smaller grain size #2135 or #4735. The resistivities measured for the stage III $CuCl_2$ compound are 3-5 times lower than values for pressed pristine KS75B powder recorded by Glenn Davis in earlier work here.

1. Pulsed Pressure Results

As seen in Tables 3 and 4, the use of pulsed pressure yielded compacts with slightly lower resistivities and slightly higher densities than those made from the same material by the constant pressure for half a minute method. This seems to conform with the idea that the pulsed pressure would allow for better rearrangement of the powder particles due to the occasional relief of pressure during the preparation procedure.

2. Annealing Results

When the compacts that were made from stage II SbF_5 powder and annealed in an SbF_5 vapor were removed from the ovens after 24 hours, there was evidence that the powders had de-intercalated. First of all, there was a white film on the inside of each glass sample holder. This is evidence

Table 6. Compact results.

Material	Stage and Intercalant	Pressing Force (Klb)	Time (min)	Temp (°C)	Resistivity (μΩ-cm)	Density (mg/mm^3)
#4735	Pristine	4	.5	25	580±150	1.97±.05
#2135	Pristine	4	.5	25	850±90	2.04±.03
#2135	Pristine	2	.5	25	1020±130	2.03±.02
#2135	Pristine	2	20	25	1200±200	2.01±.02
#2135	Pristine	2	20	175	860±90	2.09±.02
#2001	Pristine	4	.5	25	320±20	2.12±.02
#4735	II SbF_5	4	.5	25	290±10	2.71±.04
#2135	II SbF_5	4	.5	25	360±40	2.74±.06
#2001	I SbF_5	4	.5	25	130±20	2.73±.02
#2001	II SbF_5	4	.5	25	101±4	2.54±.05
#2001	II SbF_5	2	.5	25	109±7	2.55±.07
#2001	II SbF_5	2	20	25	108±4	2.63±.05
#2001	II SbF_5	2	20	175	111±5	2.55±.06
#2001	III SbF_5	4	.5	25	89±3	2.36±.05
#2001	IV SbF_5	4	.5	25	108±5	2.34±.02
KS75B	III $CuCl_2$	4	.5	25	560±70	2.32±.03
KS75B	III $CuCl_2$	2	.5	25	700±100	2.17±.03
KS75B	III $CuCl_2$	2	20	25	470±90	2.24±.05
KS75B	III $CuCl_2$	2	20	175	340±20	2.27±.07

of HF, a common SbF_5 de-intercalation product, interacting with the pyrex. Also, the resistivities increased from the original pre-annealing values by factors of 2-3, almost to levels corresponding to compacts made of pristine powders of the same particle size.

Similar results were achieved when the stage III $CuCl_2$ compacts were annealed. Deposits were seen on the tube walls of those samples fired at 300°C, but not those at 200°C. However, all the resistivities increased by 2½ to 3½ times their original values.

In both sets of annealing experiments, it was assumed for the calculation of the final resistivities that the thickness did not change throughout the process. Given the sometimes violent nature of the de-intercalation process, this assumption may not be very valid. In any case, annealing did not give the desired result of lower resistivities.

3. High Temperature Pressing Results

There was no effect on either resistivity or density caused by heating compacts as they were pressed when the stage II SbF_5 powder was used. This is not the case with the stage III $CuCl_2$ powder as can be seen in Fig. 23. There are clear correlations between the length of time the compacts

Fiq. 23 Density and resistivity vs. time of applied pressure at high temperature (175°C).

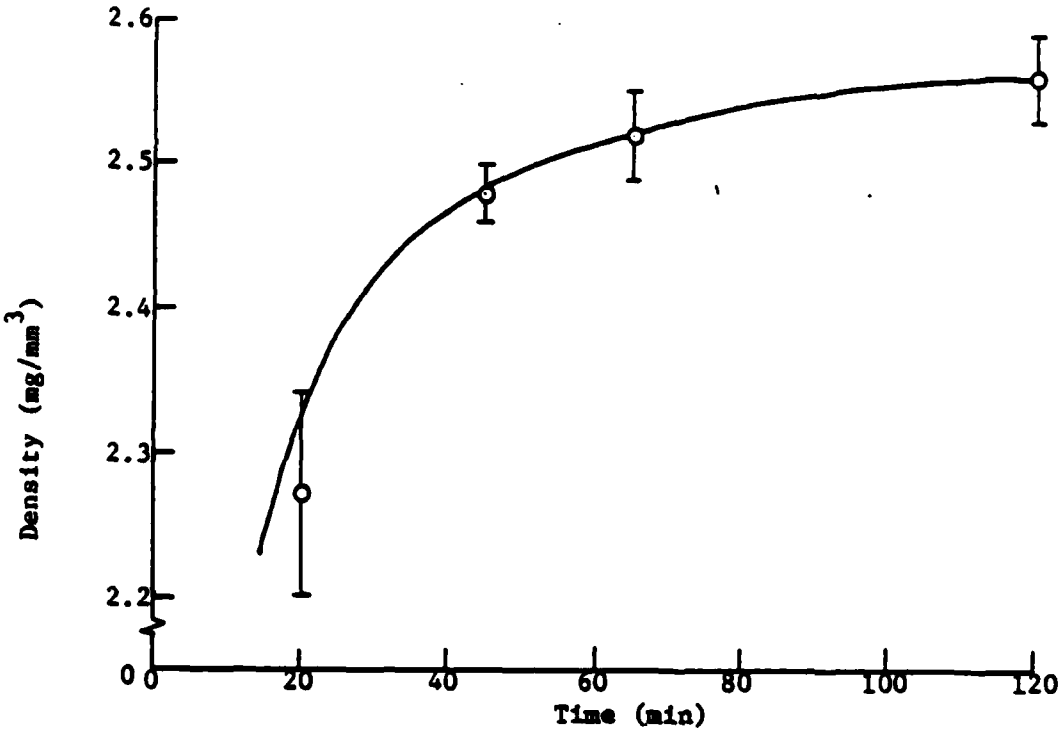

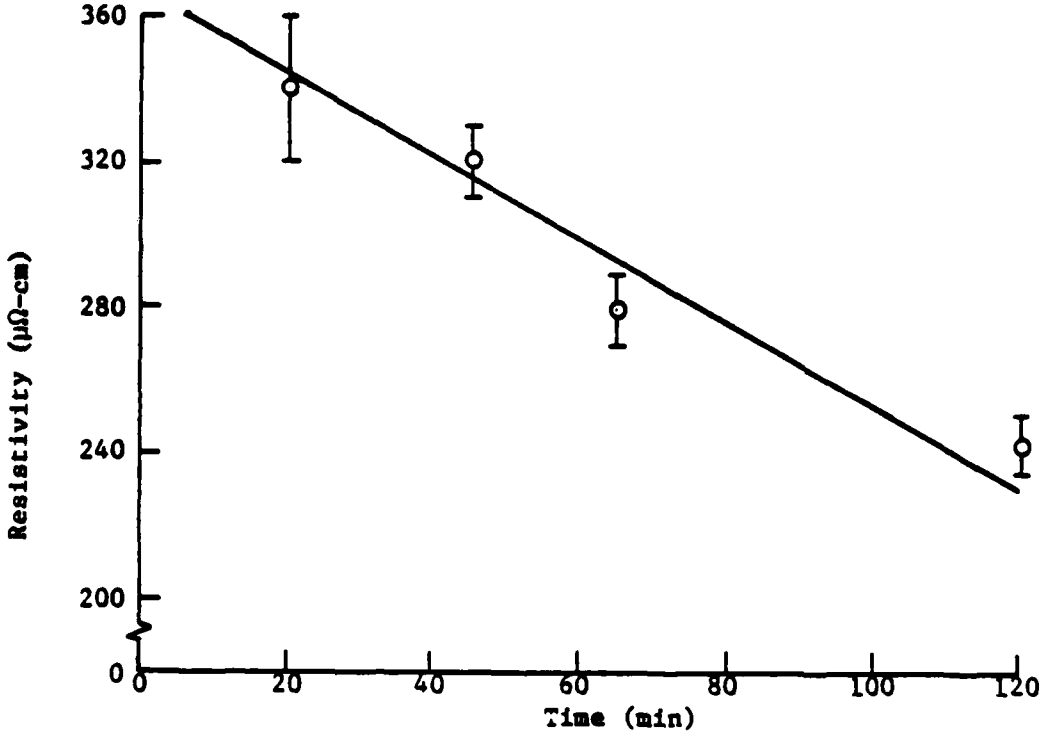

were heated and pressed and the resulting densities and resistivities.

The X-ray diffraction spectra taken of graphite samples before and after compact production showed no differences at all. Since the intercalation properties of the graphite had not been altered, it can be concluded that heat and pressure over time led to better orientation of the powder particles.

This settling could involve a higher degree of ordering of the c-axes of the individual particle crystals as well as an increased contact area between powder particles. Both of these would cause an increase in the conductivity of the compacts as measured with the contactless induction apparatus.

There was very little change in density or resistivity when pressing compacts from stage III $CuCl_2$ or pristine #2135 at 2 Klb at room temperature when the time of pressing was increased from ½ minute to 20 minutes. However, there is a substantial difference when comparing results for pressing at 2 Klb for 20 minutes at room temperature and at 175°C. (See Fig. 23.)

There is something about the higher temperature which seems to make graphite flow and settle easier. This was noticed in the first attempt at heating when the graphite flowed into the press fusing it together. This tendency to flow when heated results in compacts of higher density and lower resistivity when pristine #2135 or stage III $CuCl_2$ graphites are used. On the other hand, there is no effect evident when the compacts are prepared from the stage II SbF_5 compound powder. This can be explained by noting the difference in particle sizes involved.

The #2001 graphite used in the SbF_5 compound has a much larger particle size than the other two. It may be that the additional degree of packing and settling which results from heating these latter powders has already been achieved in the compacts prepared at room temperature from the larger size #2001 compound. The added time and heat would then not have the desired effect on these already packed compacts.

D. Conclusions

It is evident that particle size has the greatest influence on the conductivity of the pressed powders. Compacts made from smaller size particle powder will have

greater total particle surface area. The greater surface area without necessarily greater contact area between particles leads to a greater number of scattering sites. This in turn causes a higher resistivity by decreasing both carrier concentration and carrier mobility.

Only when powders are of the same size can comparisons be made on the other factors involved in compact production. For SbF_5 intercalated graphite, the best conductivities (i.e. the lowest) were found using powders prepared for stage III. The effects of heat and pressure over time were more mechanical in nature than chemical. There was no evidence that the state of the intercalation of the powders changed during the compact production process. Rather, the heat and pressure at times led to better packing of the powders into denser more conductive compacts.

Due to the range of pressures that are available using a Buehler press, only the tail end of the obvious pressure dependence of compact resistivities can be seen. Most of the working pressures for the press are above the suggested pressure saturation levels for these graphites.

On the other hand, it is also possible that the compacts would not have been sturdy enough had they been prepared at lower pressures. This is likely the case for the pristine

graphites which tended not to hold together as well as the intercalated powders.

V. Investigation of Electrical Resistivity of SbF_5 Intercalated Graphite as a Function of Temperature and Structure

A. Introduction

Of fundamental importance to the electrical conductivity of any conducting material are the conductivity mechanisms in the crystal itself. These are strongly influenced by temperature and structure which makes those variables the ones of prime concern in this study. Antimony pentafluoride was chosen as the intercalant because the highest electrical conductivity was reported for this compound (5, 11).

In the course of investigating the temperature dependence of resistivity a cooling rate sensitive order-disorder transformation was observed.

These phase transitions in graphite intercalation compounds (GICs) are very interesting in a scientific point of view, because the phenomenon is nearly two-dimensional. In GICs, the in-plane structure of the graphite layer remains the same as that of host graphite, but the in-plane structure of the intercalant layer depends on the intercalant species and the temperature. Order-disorder transition in GICs has been observed in both donor compounds and acceptor compounds. For the case of donor compounds, in addition to the in-plane ordering (C_6M or C_8M), there is also inter-plane ordering ($\alpha A\beta A\gamma A\delta A...$)(16, 17, 18, 19) for the intercalant layers, where A represents the graphite layer and α,β,γ and δ are

the intercalant layers. For acceptor compounds, the intercalant layer is often disordered or liquid-like at room temperature, and has an ordered structure at low temperature (20, 21, 22). The transition to ordered behavior has been studied by x-ray (22), neutron (22) and electron diffraction (20) and the consequences of the order-disorder transition have been observed in basal plane transport properties (23, 24) and NMR (25, 26). No single compound has been systematically studied by a variety of techniques, however. The order-disorder transition of SbF_5-graphite has been reported by an NMR experiment (26) on SbF_5-intercalated graphite powder, which gives the transition temperature at 190K for $C_{27}Sb_5$.

In these experiments, the phase transition of SbF_5-graphite is investigated with samples of SbF_5-intercalated HOPG (Highly Oriented Pyrolitic Graphite). Three different experiments have been employed to study this phenomenon: (1) electrical resistivity measurements; (2) differential scanning calorimetric (DSC) measurements and (3) the in-plane structure analysis with an Energy Dispersive X-ray Diffraction (EDXD) system. All three experiments give consistent results on the transition temperature. An in-plane structure of the intercalant layer, which rationalizes all three measurements, is proposed.

B. Experimental Work

1 Sample Preparation

HOPG from the Union Carbide Corporation was cut with a diamond blade into 5 mm x 5 mm squares and was cleaved normal to the c axis to a thickness of approximately 0.1 - 0.2 mm. This sample geometry was chosen because the r.f. induction method used to measure the resistivity of the samples is well calibrated for these dimensions. After the dimensions, weight and room temperature resistivity had been recorded, the sample was loaded into the side arm of the h-shaped Pyrex tubing shown in Fig. 24. The two round rods attached at the diagonal corners of the 2 mm x 6 mm rectangular tube enable the sample to be placed either at an angle to the glass surface for x-ray diffraction and optical reflectivity measurements of flat on the surface of the glass tube for resistivity measurements.

SbF_5 from Ozark Mahoning was loaded into the other arm of the h-shaped tubing inside the glove box with an argon gas atmosphere. After pumping out the argon gas, the tube was sealed by a torch at the dent mark shown in Fig. 24. The tube was then turned upside down and the side with SbF_5 was placed in a constant-temperature bath of temperature T_1 while the side containing the sample was put into a tube furnace of temperature T_2. The set-up for the intercalation process is shown in Fig. 25.

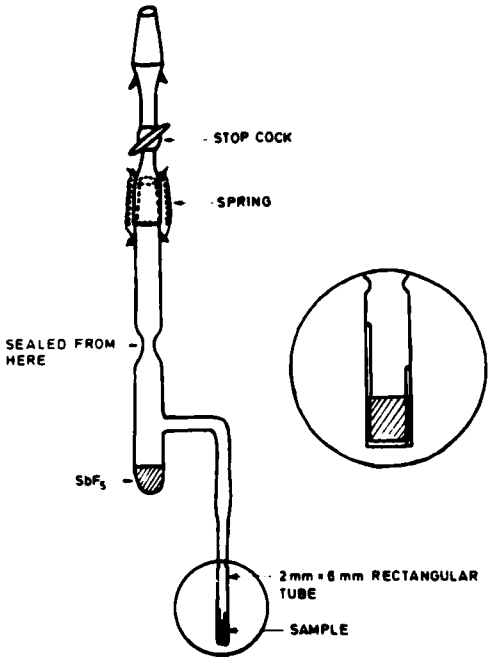

Fig. 24. h-shaped Pyrex tubing for the SbF_5-HOPG intercalation process.

By controlling the temperature T_1 we can control the vapor pressure of SbF_5 around the sample, which in turn determines the stage of intercalation. Figure 26 gives the experimental data showing the stage of intercalation plotted against T_1 and T_2 is held at around 90°C. Similarly by changing the reaction temperature T_2, we can control the reaction rate of the intercalation process and thereby also control the stage of intercalation. Figure 27 shows the results of stage plotted against T_2 where T_1 is held at 10°C. Either method can yield a good quality sample

from stage 1 to stage 4. No sample with a pure stage higher than stage 4 has been made, however, because (1) the temperature range (T_1 and T_2) required to obtain stage 5 is so narrow that more accurate temperature control is necessary and (2) the reaction rate is very slow (the reaction time is in the range from 6 months to 1 year).

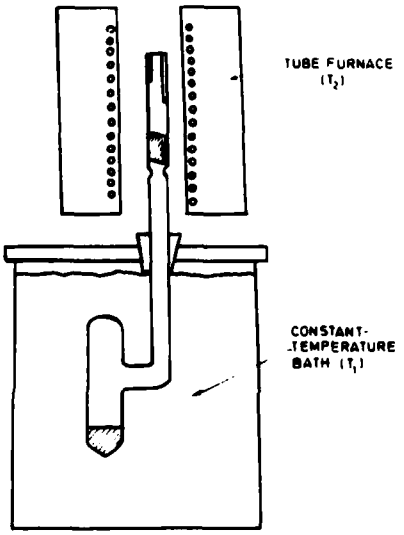

Fig. 25. Two-temperature-zone method for SbF_5-HOPG intercalation.

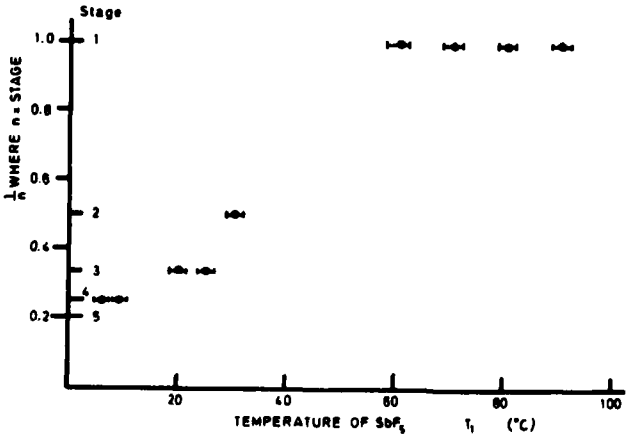

Fig. 26. Stage of intercalation v.s. T_1 (the temperature of SbF_5) when T_2 (the reaction temperature) is held at $^{2}90^{o}C$.

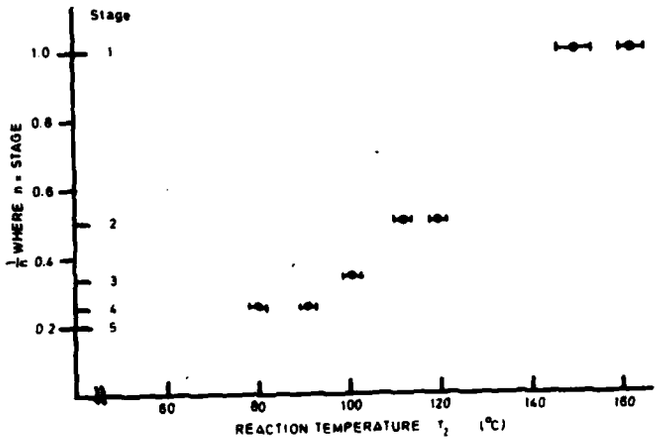

Fig. 27. Stage of intercalation vs. T_2 when T_1 is held at 10°C.: vapor pressure of SbF_5, 1.6 Torr.

B-2 Characterization of the Sample

a. X-ray diffraction

The stage of intercalation and the c axis repeat distance are determined by the (00ℓ) reflections of Mo Kα radiation. The measurements made <u>in situ</u> allow us to monitor the progress of the intercalation process and to stop the reaction by sealing off the sample from the h-shaped tube. Since the samples are thin enough to be comparable with the penetration depth of the Mo Kα radiation, the diffraction peaks indicate the purity of the sample in the intercalation stage. Figures 28, 29, 30, and 31 are the diffraction charts of samples of stages 1, 2, 3, and 4 respectively. The sharpness and strength of the peaks indicate that all the samples are single stage and of good quality. The repeat d spacing along the c axis was calculated by fitting 1/D

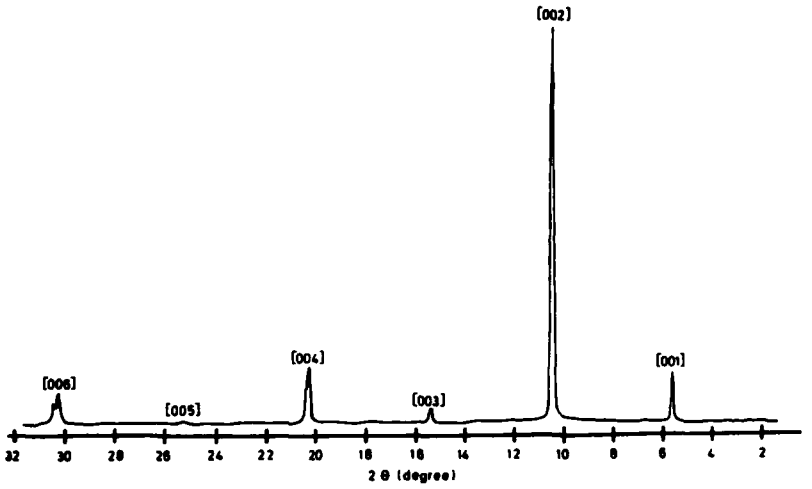

Fig. 28. 00ℓ diffraction for Mo Kα radiation on stage 1 graphite-SbF_5.

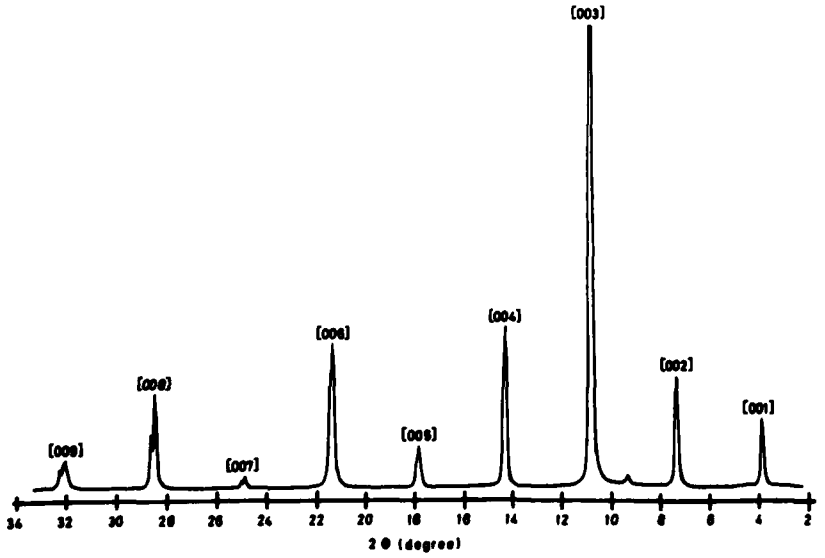

Fig. 29. 00ℓ diffraction for Mo Kα radiation on stage 2 graphite-SbF_5.

against θ with a least-squares program yielding the results given in Table 7. These data agree very well with the data reported previously in the literature on intercalated graphite powder (27).

Table 7
Resistivity and plasma frequency of SbF_5-graphite

Stage	*n in C_n–SbF_5*[a]	d_i[b] (Å)	*Room temperature resistivity* ρ ($\mu\Omega$ cm)	*Plasma frequency* ω_p (eV)
1	8.5 - 9.0	8.33 - 8.37	2.90 - 3.50	1.85
2	≈18	11.67 - 11.75	2.50 - 3.50	1.55
3	≈27	15.00 - 15.10	2.80 - 3.10	1.31
4	≈35	18.40 - 18.55	2.25 - 3.05	1.2

[a]Values taken from the gravimetric measurements on the assumption that the intercalant is SbF_5.
[b]d_i, repeat *d* spacing along the *c* axis.

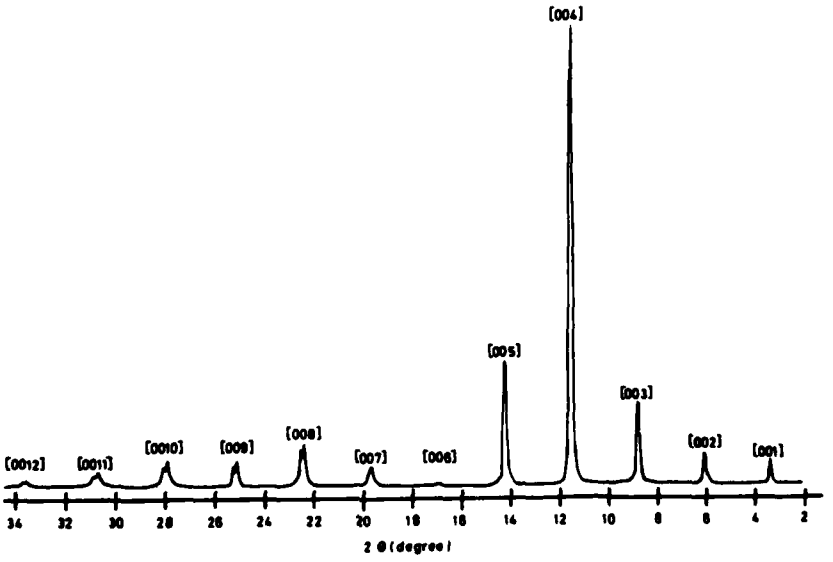

Fig. 30. 00ℓ diffraction for Mo Kα radiation on stage 3 graphite-SbF_5.

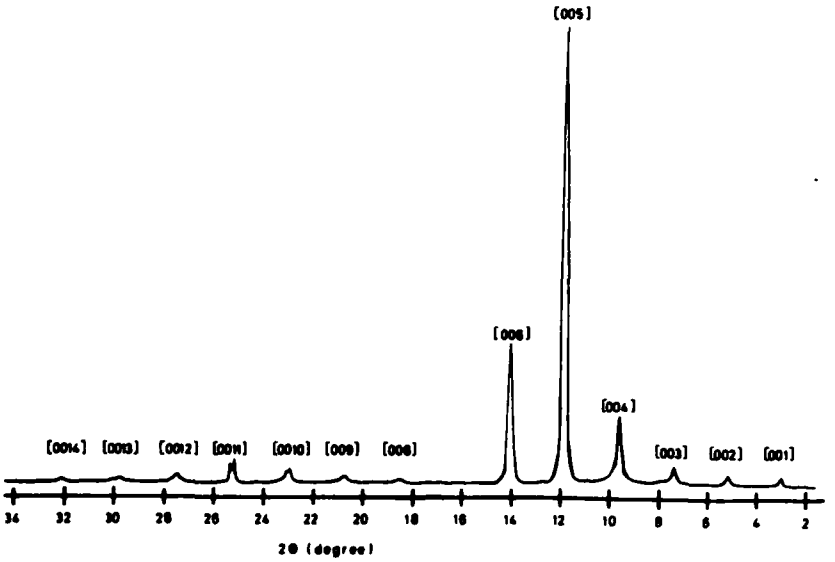

Fig. 31. 00ℓ diffraction for Mo Kα radiation on stage 4 graphite-SbF_5.

b. Optical reflectance experiments

As for graphite intercalated with AsF_5 (28) the color of the sample is blue for stage 1 and black for all other stages. The higher the difference between T_1 and T_2 during the intercalation process, the better is the surface for optical measurements. Optical reflectance measurements were made with near-normal incidence on c faces, and hence with light polarization perpendicular to the c axis ($e \perp c$) of the samples. Reflectances were measured either in situ or after x-ray analysis had shown the sample to be a pure single stage. The curves of stages 1-4 are shown in Fig. 32. The plasma frequencies ω_p determined from the minimum in the reflectance curve are listed in Table 7, fifth column. The data are in good agreement with those reported previously (29).

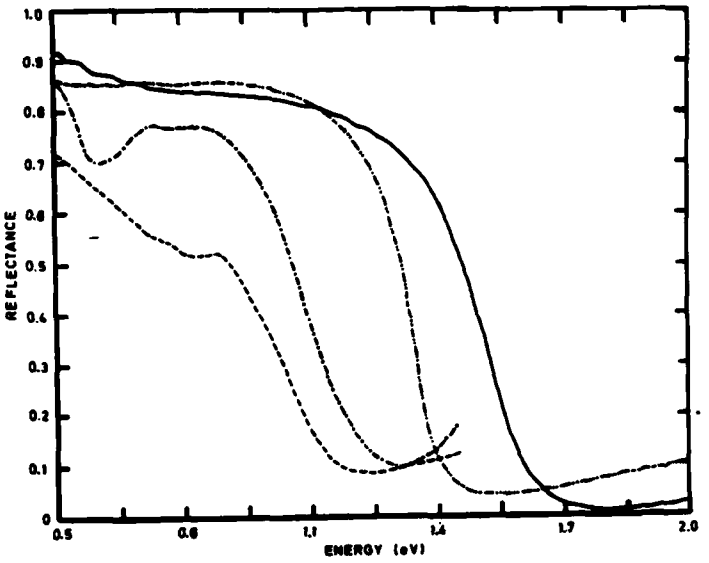

Fig. 32. Reflectance of SbF_5-graphite for stages 1(——),2(-·-·-·-),3(-··-··-) and 4(- - -).

c. Room temperature resistivity measurements

The conventional four-point contact method for measuring the resistivity is not suitable for our samples because (1) a large c axis expansion (d_i = 8.33 Å) makes it difficult to maintain good contacts to the sample, (2) the high anisotropy ($\rho_c/\rho_a > 10^6$) (28, 30) prevents unevenly injected current from distributing itself over reasonable sample geometry and (3) the material to be intercalated (SbF_5) is corrosive. To overcome these difficulties, a ferrite core r.f. induction method (31) has been developed to measure the resistivity of samples at room temperature. The system operates at 1 kHz where, for conductivities comparable with copper, the skin depth is about 2 - 3 mm which is much larger

than the thickness of the samples. After calibrating with a series of samples with known resistivity, we obtained an empirical equation for the system:

$$\rho = \frac{kes^2}{\Delta V} \qquad (1)$$

where ρ is the resistivity of the sample in micro ohm centimeters, k the constant of the ferrite core system (=0.122 at 22°C. for a 5 mm x 5 mm sample), e the thickness of the sample in millimeters, s the surface area of the sample in square millimeters and ΔV the measured voltage change in millivolts.

d. Measurements of temperature dependence of resistivity

Using the r.f. eddy current technique (32) in conjunction with cryogenic systems, we can measure the resistivity of a sample from 4.2 to 300 K. At low temperatures since the empirical equation (1) holds for this system only the constant k is different.

e. Differential scanning calorimetry (DSC)

Whenever an order-disorder phase transition occurs in a material, some change in the thermal properties should be observed either in specific heat, C_p, or in enthalpy, ΔH, on passing through the transition temperature. Differential scanning calorimetric (DSC) measurements were used to study the phase transition in stage one SbF_5-graphite. Measurements were done with a DuPont 990 Thermal Analyzer together with a DuPont DSC Cell (catalog No. 900600-902).

Each sample used in this experiment was weighed and loaded into a covered pan provided with the equipment. A special press was used to seal the pan. For air-sensitive materials, such as SbF_5-graphite, all the procedures mentioned above were carried out inside a glove box with an inert gas atmosphere. The seal of the pan was found to be air-tight by checking the sample after the measurements. The sample of stage 1 of SbF_5-HOPG retained its shiny blue color as the pan was opened. During the measurement, the sample was put on the sample platform of the DSC Cell, with an empty pan at the reference platform. The whole DSC cell was then cooled down to the temperature at which the measurement was begun. The most rapid cooling rate feasible in this system was 5 to 10 degrees per minute. Therefore, only measurements associated with the slowly cooled case in resistivity measurements could be made. All the measurements were done under heating from -130° (143K) to 25° (298K) with a heating rate of 5 degrees per minute. Three different sample pans were measured, one empty pan, one loaded with 19.5 mg of HOPG and one loaded with 25.7 mg of stage I SbF_5-HOPG.

f. Energy dispersive x-ray diffraction (EDXD)

Even though the order-disorder phase transition has been observed in various experiments on different acceptor compounds, the structure of the intercalant layer in the ordered phase and the change of the structure while the material undergoes a phase transition are still largely unknown. In another experiment, an Energy Dispersive X-ray

Diffraction (EDXD) system was used to study the in-plane structure of the intercalant layer at various temperatures. Unlike the conventional angular-scanning diffraction source, the EDXD method utilizes white x-radiation and a fixed diffraction angle. At a fixed angle, the scattering vector is proportional to the energy of the incident photon. Therefore, the diffracted intensity spectrum (as a function of energy) contains the same structure information as can be obtained by conventional diffraction measurements (32, 33). The expression for Bragg diffraction is:

$$2d \sin \theta = n \frac{12400 \ (\text{Å})}{E} \qquad (2)$$

where d = d-spacing of the diffraction plane in Å

θ = incident angle of the x-ray with respect to the diffraction plane

n = order of the diffraction

E = energy in eV.

Figure 33 is the schematic drawing of the EDXD system used in this experiment. The tungsten target (W-target) x-ray tube was operated at 48 kV (10^3 volts), with a beam current of 14 or 20 mA (full wave). Therefore, the full spectrum of output covers up to 48 keV. An intrinsic germanium (Ge) detector (Princeton Gamma-Tech) was used as the detector. A pulse pileup rejector and a pulse shaper were added to improve the accuracy of counting at higher counting rates. The data were fed into a multichannel pulse height analyzer (MCA). The channel width of the MCA was

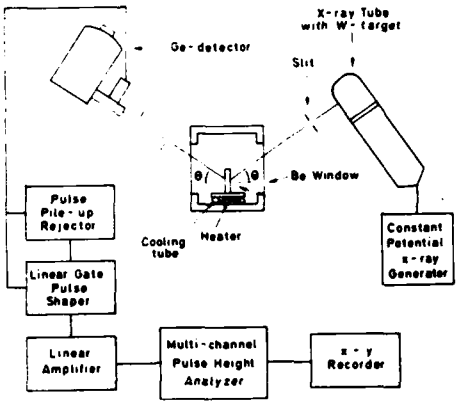

Fig. 33. Schematic drawing of energy dispersive x-ray diffraction (EDXD system).

usually set to 100 eV, so that 500 channels covered the entire spectrum. The sample was loaded in a brass cell with two beryllium (Be) windows as shown in Figure 33. Cooling of the sample was accomplished by passing cold nitrogen gas through the cooling tube, and fine temperature control was achieved by a temperature controller (Lake-Shore DRC-70C) which supplied current through the heater in the cell.

To study the in-plane structure of the intercalant layer, the momentum transfer, $\vec{q}$, of the x-ray is perpendicular to the $\vec{c}$-axis of the sample. There are two ways of arranging the sample with respect to the incident and the diffracted beams to satisfy this requirement: (1) the plane defined by the incident and the diffracted beams (the plane of incidence) is perpendicular to the $\vec{c}$-axis (2) the plane of incidence is parallel to the $\vec{c}$-axis. In the former, the detector picks up the reflected beam while for the latter the detector picks the transmitted beam. For GICs it is very difficult to obtain a large and plane a-surface (surface $\parallel$ the $\vec{c}$-axis) so that method (1) is impractical. Fortunately, it is easy to

prepare very thin samples for GICs so that method (2) can be used successfully. Samples for this experiment were prepared with dimensions of 8 mm x 8 mm x 0.2 mm for ease of alignment.

The output spectrum of this experiment contained two kinds of peaks: (1) fluorescence peaks whose positions (in energy) were independent of θ (angle of the incident beam (2) Bragg peaks whose positions were dependent on θ according to Eq.(2). Therefore, as the angle was changed, the Bragg peaks, unlike the Fluorescence peaks, would move to other energies. After a series of angles was tested, θ= 9 degrees was selected as the best position to observe the structure change of the intercalant layer.

C. Results

1. Resistivity

Figure 34 shows the results of the resistivity plotted against the stage at room temperature for all the samples which were measured. All the points are from samples which x-ray analysis shows to be a pure single stage. The limits of error correspond to the size of the circles of the data points and the systematic errors tend to underestimate the conductivity. Therefore in Fig. 34 the scattering of the data points is caused by variation in individual samples and a broken line is drawn through the maximum conductivity to indicate the trend (28). The full circles are for the samples used to measure the temperature dependence of resistivity.

In. Fig. 36 we present the plot of the signal from the 1 kHz air coil r.f. system of Fig. 35 vs. the signal from the 1 kHz ferrite core r.f. system, both at 22°C. A straight line passing through the origin shows that the two systems are perfectly comparable. Another feature of the air coil r.f. system is that it can operate at any frequency of the oscillator and the lock-in amplifier. The operating frequency is determined by optimizing between the skin depth effect and the detectable signal. The curve shown in Fig. 37 of an HOPG sample measured to verify the system agrees very well with the contact bridge measurements (34, 35).

Subsequent to the discovery made while making measurements on acceptor compounds that the curves of resistivity against

temperature differed according to whether the samples were slowly cooled or quenched, the following procedures were established.

(1) Each sample was quenched from room temperature to 77 K, at a rate of about 50 K min^{-1}.

(2) The sample was held at 77 K overnight to reduce transient effects.

(3) The sample was cooled to 4.2 K by transferring liquid helium into the Dewar flask.

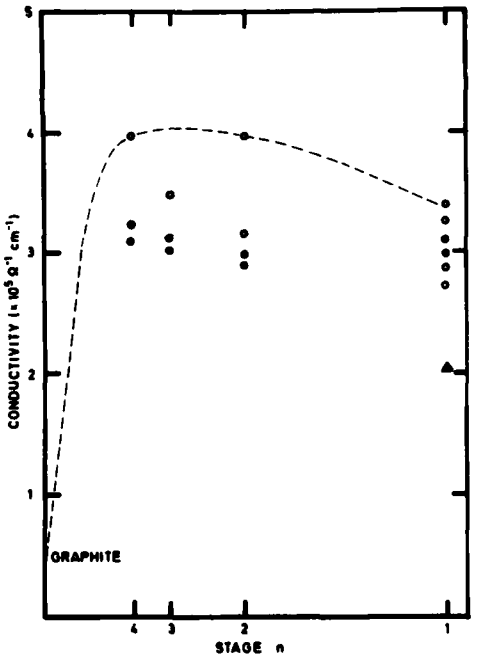

Fig. 34. Room temperature resistivity vs. stage for graphite-SbF_5:o, HOPG; Δ, natural graphite.

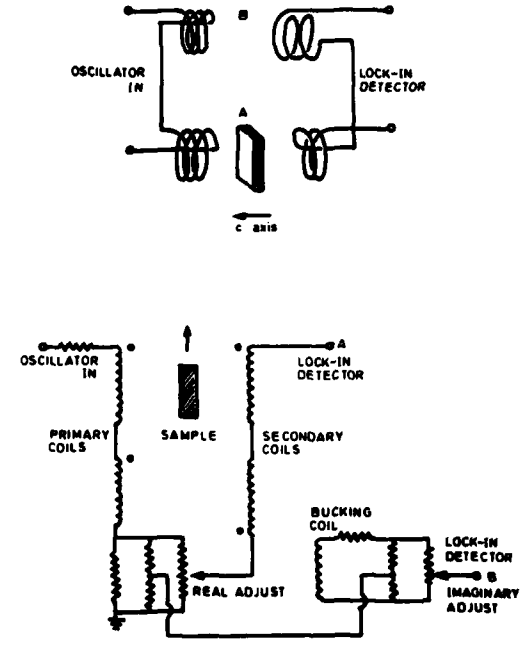

Fig. 35. Schematic diagram of the air coil r.f. induction circuit.

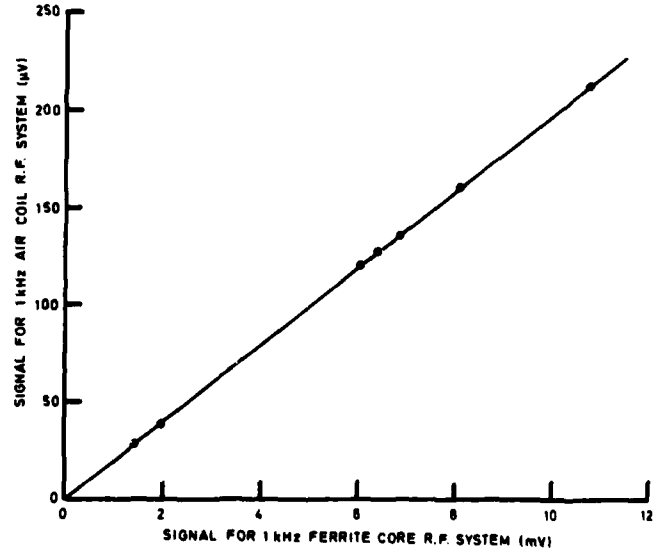

Fig. 36. Comparison of the 1 kHz air coil r.f. system with the 1 kHz ferrite core r.f. system.

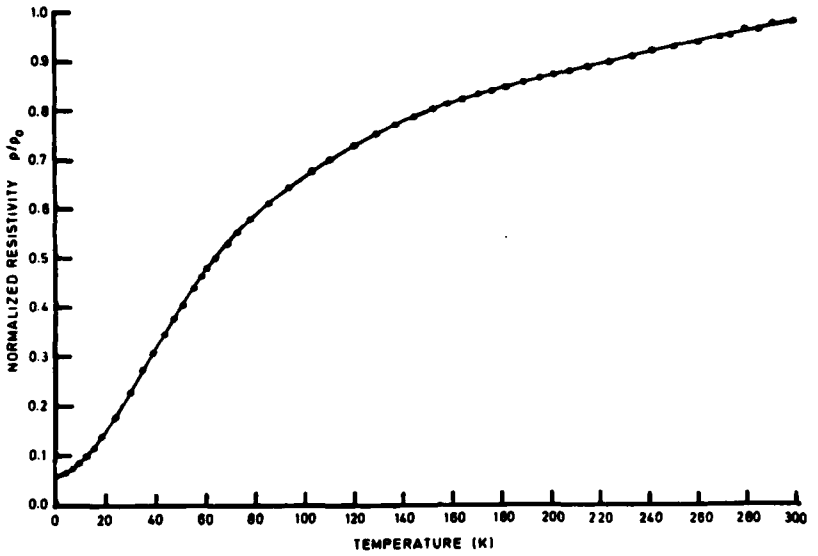

Fig. 37. Normalized resistivity vs. temperature for HOPG where ρ_0 is $\rho(T)$ at 300 K(ρ_0 = 40 μΩ cm).

(4) The temperature of the sample chamber was allowed to rise gradually from 4.2 to 77 K. At frequent intervals the signal from the thermocouple and the conductivity signal of the sample were read simultaneously. Every 5 or 10 K the coils were rebalanced after raising the sample holder 6 in out of set A.

(5) Above 77 K a cryogenic temperature controller was used to control the temperature of the sample chamber. Data were taken at intervals of 5 K from 77 K to room temperature. As the sample chamber was held steady at a given temperature tne coils were balanced and the measurements were taken. 10 - 15 min. were required to take each point.

(6) After the sample had reached room temperature, it was slowly cooled to 77 K at a rate of about 100 K h^{-1}.

(7) The same procedures (2) - (5) were repeated to

measure the signal and the temperature of the sample.

The measurements of stages 1, 2, 3 and 4 of SbF_5-intercalated HOPG are shown in Figs. 38, 39, 40 and 41 respectively. The broken curves are plots of the resistivity against temperature as the sample was quenched during the cooling procedure and the full curves are the intrinsic temperature dependence of resistivity.

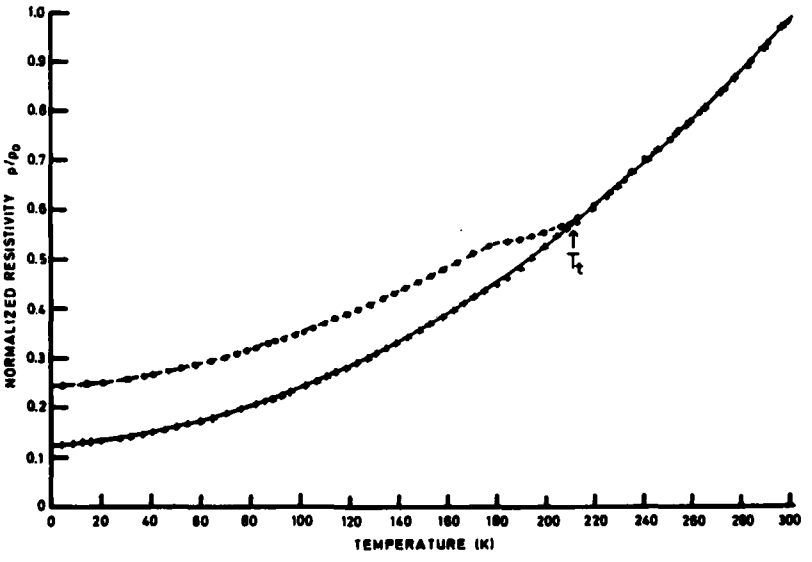

Fig. 38. Normalized resistivity vs. temperature for stage 1 graphite-SbF_5 where ρ_0 is $\rho(T)$ at 300 K (ρ_0 = 3.28 μΩ cm): +, slowly cooled; •, quenched.

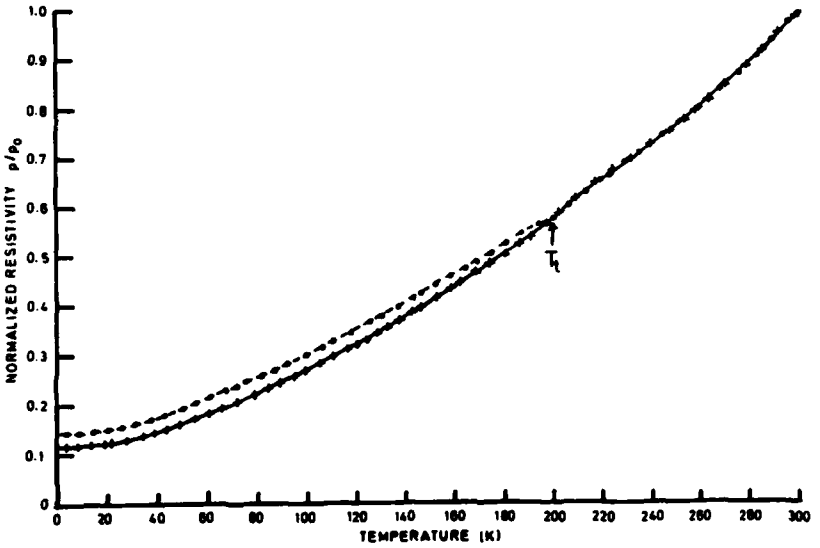

Fig. 39. Normalized resistivity vs. temperature for stage 2 graphite-SbF_5 where ρ_0 is $\rho(T)$ at 300 K (ρ_0 = 3.42 μΩ cm): +, slowly cooled; •, quenched.

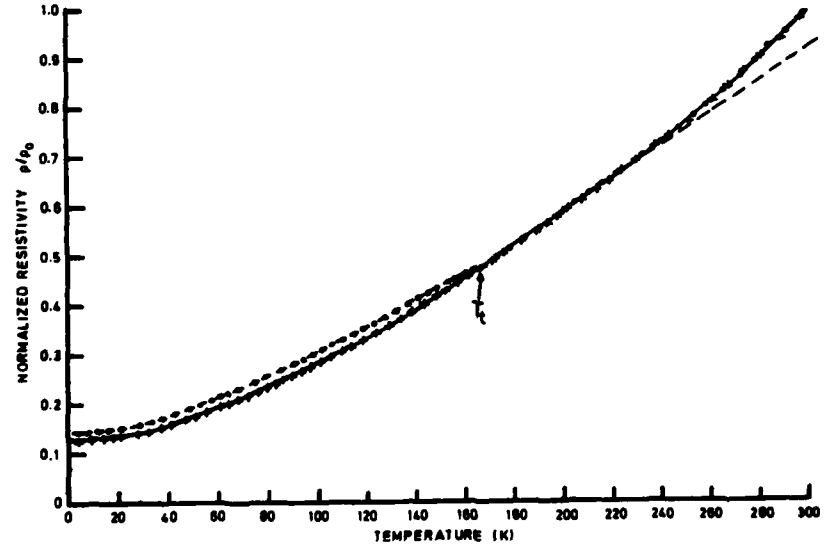

Fig. 40. Normalized resistivity vs. temperature for stage 3 graphite-SbF_5 where ρ_0 is $\rho(T)$ at 300 K (ρ_0 = 3.24 μΩ cm): +, slowly cooled; •, quenched.

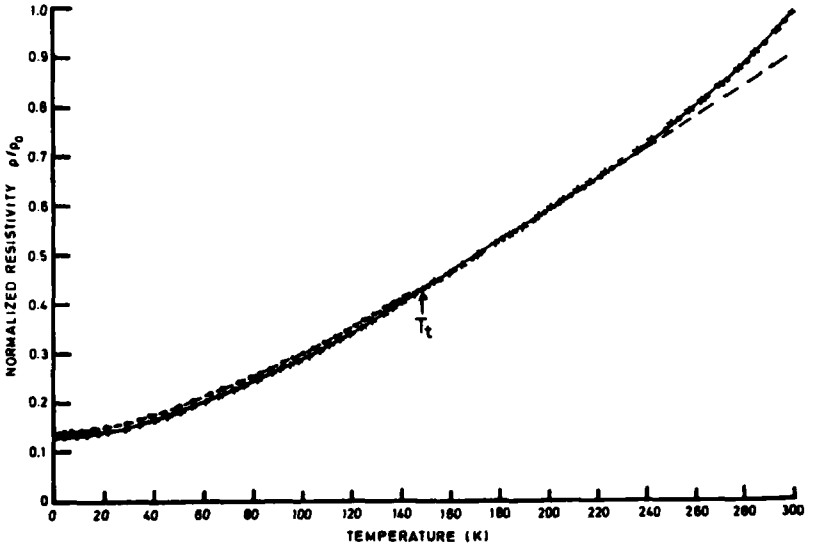

Fig. 41. Normalized resistivity vs. temperature for stage 4 graphite-SbF_5 where ρ_0 is $\rho(T)$ at 300 K (ρ_0 = 3.21 μΩ cm): +, slowly cooled; •, quenched.

2. Differential scanning calorimeter

These results are shown in Figure 42. A broad transition is observed for the stage 1 sample. The values of T_ℓ and T_u were found to be 189K and 217K, which agreed well with the data from resistivity measurements (Table 8).

From Figure 42, the specific heat, C_p, for HOPG and stage 1 SbF_5-HOPG can be calculated using the following expression (36).

$$C_p = \frac{60\ E \cdot \Delta q}{H_r \cdot m} \qquad (3)$$

where C_p = specific heat (cal/g-°C.)

E = DSC cell calibration coefficient at the temperature

H_r = heating rate (°C. per minute)

Δq = Y-axis displacement between the sample curve and reference on (empty pan) in 10^{-3} cal/sec

m = sample mass (mg)

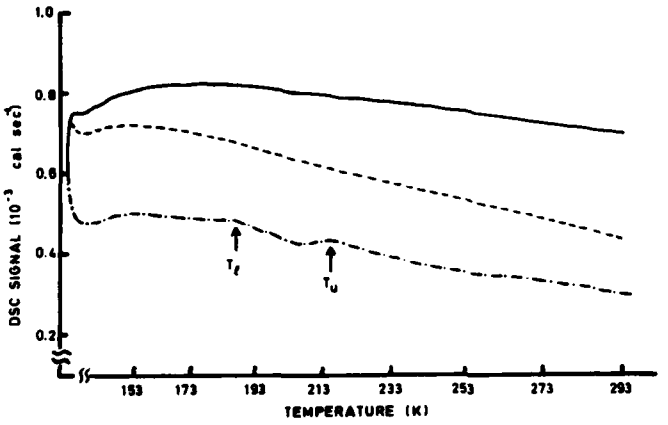

Fig. 42. Data of DSC measurements: (1) an empty pan, (2) a pan loaded with 19.5 mg HOPG and (3) a pan loaded with 25.7 mg stage 1 SbF_5-HOPG.

The value of E (DSC cell calibration coefficient) is usually close to 1.0 and can be determined by measuring some known materials. If the value E = 1.0 is used in our calculation, the values of the specific heat for HOPG and stage 1 SbF_5-HOPG will be the result shown in Figure 43. At 20°C. (293K) the value of C_p for HOPG was calculated to be 0.16 cal/g-°C., which is very close to the handbook value of 0.17 cal/g-°C. (37).

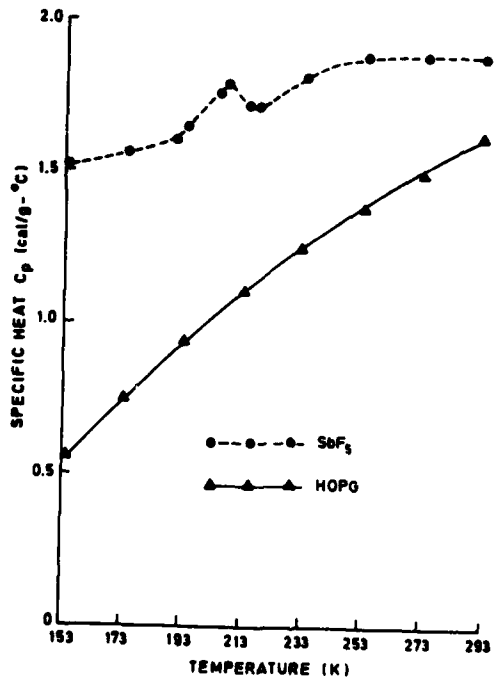

Fig. 43. Specific heat (C_p) for HOPG and stage 1 SbF_5-HOPG.

3. X-ray results

Two kinds of samples were measured, HOPG and Stage 1 SbF_5-HOPG. For the HOPG sample, the spectrum was found to be independent of temperature; the spectrum was the same at both 295K and 165K, as seen in Figure 44. With the plane of incidence parallel to the $\vec{c}$ axis, the hko Bragg peaks of graphite were observed as shown in Figure 44. The broad peak around 22.4 keV is the 110 peak shifted by the Kα line of Ge about 2 to 3% of the original peak in intensity. The peaks between 8 keV and 10 keV are peaks associated with the fluorescence lines of tungsten (W) and the 100 peak shifted by Ge in the detector.

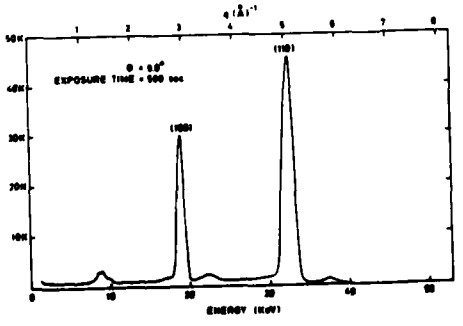

Fig. 44. EDXD spectrum for HOPG (both at 165 and 295 K).

For stage one SbF_5-HOPG, the results are shown in Figures 45 and 46 with respect to temperatures below and above the transition temperature (T_t). In addition to the Bragg peaks of graphite and the fluorescence lines of Sb, W and Pb (Sb in the sample, W from the x-ray source and Pb from the slits) there were two sets of Bragg peaks associated with the in-plane structure of the intercalant layer. One set, which had the strongest peak at 20.7 keV, lost intensity above 185K, while the other set, which had a strong peak at 22.4 keV, remained at the same intensities for all temperatures. Figure 8 is a plot of intensity vs. temperature for three different peaks at 6000 seconds counting time. The numbers 1 to 10 on the figure represent the sequence of the data taken. The intensities of the graphite 110 peak (32.0 keV) and the peak at 22.4 keV were independent of temperature, but the peak at 20.7 keV underwent a sharp step at around 185K. This indicates that there is a definite structural change in the intercalant layer around 185K, which was just the temperature of the anomalies observed in the other two experiments as seen in Table 1. Therefore, we concluded that the phase transition in SbF_5-graphite was an order-disorder process of the intercalant species. The detailed mechanism of this ordering process will be discussed later.

From Figures 45 and 46, some information about the in-plane structure of the intercalant layer could be obtained by analyzing the Bragg peaks due to the intercalant layers. Since the whole spectrum contains the fluorescence peaks and

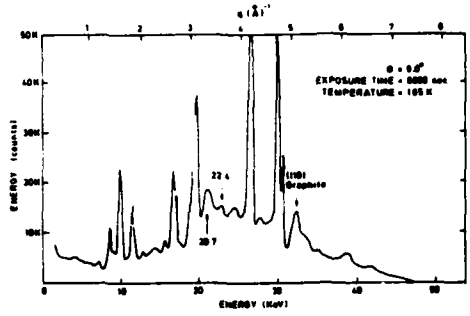

Fig. 45. EDXD spectrum for stage 1 SbF_5-HOPG below the transition temperature.

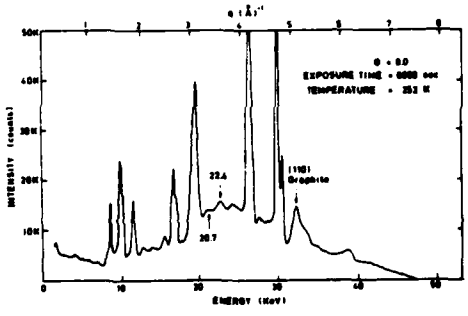

Fig. 46. EDXD spectrum for stage 1 SbF_3-HOPG above the transition temperature.

the Bragg peaks, it is necessary to know the locations of the fluorescence peaks first. The major elements in our samples are carbon (C), fluorine (F) and antimony (Sb). Carbon and fluorine are very light atoms so that their fluorescence lines are at very low energies (below 1 keV). The major fluorescence lines of antimony are the Kα and Kβ lines which are located at 26.1 and 29.7 keV, respectively. For any strong peak in the spectrum, there are peaks (about 2 to 3% of the original peak in intensity) caused by the Kα and Kβ of Ge (in Ge detector). The peaks shifted by the Kα and Kβ lines of Ge are 9.9 keV and 10.1 keV below the

original energies. Since the peaks at 26.1 and 29.7 are very strong, there are peaks around 16.2 keV and 19.8 keV associated with them due to the shift of the detector. The other fluorescence peaks are the $L\alpha$, $L\beta$ and $L\gamma$ of tungsten (W-target) and the $L\alpha$ and $L\beta$ of lead (from the slits) at the energies of 8.3, 9.7, 11.2, 10.4 and 12.6 keV, respectively. The additional peaks are associated with the in-plane structure of the intercalant layer.

Due to the limitation of the system and the Ge detector, the efficiency of the output spectrum is not uniform over the whole energy range. Both in the very low energy and very high energy regions, the intensity is low so that the peaks in these regions are difficult to identify. The best region in the whole spectrum is the region around 20 keV.

Table 9 lists the peaks from 7.0 keV to 30 keV. The 1-0 peak of graphite is buried under the peak at 19.6 keV, so that it is difficult to tell the exact position. All the Bragg peaks of the intercalant layer could be fitted into the following expression with ΔE = 1.75 keV:

$$E_n - n\ \Delta E \qquad (4)$$

where E_n = energy of the nth order peak

n = index of the order

ΔE = difference in energy between nth and (n+1)th orders.

The ΔE = 1.75 keV corresponds to the repeat distance of about 2.65 Å in real space. This structure existed both below and above T_t. As the Figures 45 and 46 were examined closely, the peaks at 6.9, 13.7, 20.7 and 27.6 keV were found to have

AD-A146 539 AN INVESTIGATION OF THE ELECTRICAL CONDUCTIVITY IN HIGHLY ORIENTED GRAPHI..(U) MOORE SCHOOL OF ELECTRICAL ENGINEERING PHILADELPHIA PA DEPT O.. F L VOGEL FEB 84 2/2

UNCLASSIFIED DAAG53-76-C-0061 F/G 11/2 NL

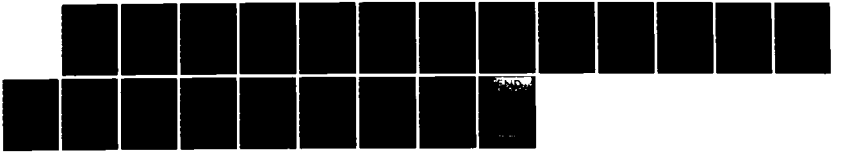

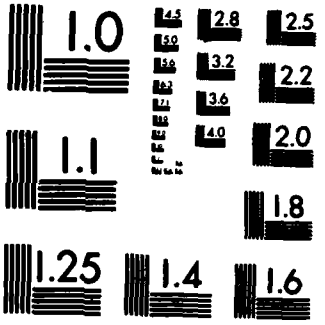

different intensities below and above T_t, especially the peak at 20.7 keV which has been shown in Figure 45. These peaks coincided with the 4th, 8th, 12th and 16th peaks of the set which was found to exist below and above T_t (d≈23 Å, ΔE = 1.75 keV). With the relation described by Eq. (4), the peaks at 6.9, 13.7, 20.7 and 27.6 could be fitted as the 1st, 2nd, 3rd and 4th orders of a set with ΔE = 6.9 keV. The peak at 20.7 keV was confirmed to be the 3rd order for the set of the peaks, that underwent intensity change at T_t, by experiments with different values of θ. Therefore, there is an ordered structure with a repeat distance equal to 5.7 Å below T_t.

Table 8. Lists of the Peaks in EDXD Measurements for Stage 1 SbF_5-HOPG

Energies of the peak (keV)	Description
6.9	Bragg peak of IL (intercalant layer)
8.3	*Lα* of W (tungsten)
9.7	*Lβ* of W
11.2	*Lγ* of W
12.6	*Lβ* of Pb (lead)
13.7	Bragg peak of IL
15.3	Bragg peak of IL
16.4	*Kα* of Sb (antimony) shifted by *Kα* of Ge (germanium)
19.6	*Kβ* of Sb shifted by *Kα* of Ge
20.7	Bragg peak of IL
22.4	Bragg peak of IL
24.0	Bragg peak of IL
26.3	*Kα* of Sb
27.6	Bragg peak of IL
29.5	*Kβ* of Sb
32.0	(110) peak of graphite
33.0	Bragg peak of IL
34.6	Bragg peak of IL
38.4	(200) peak of graphite

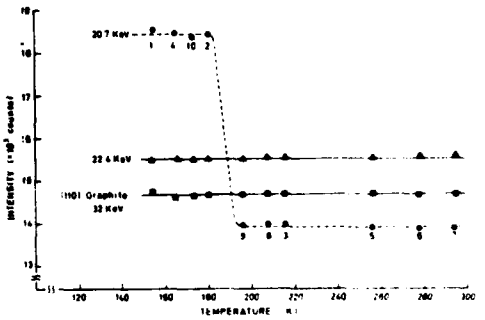

Fig. 47. Temperature dependence of intensity for three selected peaks in EDXD spectrum of stage 1 SbF_5-HOPG.

D. Discussion

The curves of resistivity against temperature for stages 1 - 4 of SbF_5-graphite have the same features with respect to the cooling rate effect. The quenched curve always has an extra residual resistivity below a certain temperature and the slowly cooled curve gives the intrinsic temperature dependence of resistivity. To understand this cooling rate effect better, an HOPG sample and a sample of HOPG intercalated with nitric acid (HNO_3) were measured with the same procedures. No noticeable difference was found between quenched and slowly cooled HOPG, which indicates that this effect is caused by the intercalant layers. Two samples intercalated with HNO_3 (one stage 2 and the other stage 4) showed the same phenomena as SbF_5-intercalated graphite. Figures 48 and 49 are the curves of stage 2 and 4 HNO_3-intercalated HOPG. The form and temperature of transition

agree well with data in the literature (37, 38). Although the hysteresis in resistivity resulting from various rates of cooling has already been mentioned (39), the "freezing-in" of an anomalously high resistive state has not been reported previously for these compounds. The results for HOPG and the two intercalated compounds (HNO_3 and SbF_5) indicate that the cooling rate effect is caused by the order-disorder transition of the intercalant layers. For most of the acceptor compounds the intercalant layer is disordered or liquid like at room temperature and is frozen below a certain transition temperature T_t. During the cooling process, if insufficient time is allowed for the intercalant to order itself, as in the quenched case, extra scattering caused by the intercalant accounts for the extra residual resistivity at low temperatures. From this argument it should be possible to observe the cooling rate effect on resistivity in most of the acceptor compounds. The temperature at which the two curves (quenched and slowly cooled) meet is associated with the order-disorder transition temperature T_t in the intercalant layer. The extra residual resistivity $\Delta\rho$ caused by the quenched case can be explained by the scattering of the disordered intercalant layer due to overlap of the wavefunctions in the intercalated and graphite layers or to strain induced by the disorder. The T_t and $\Delta\rho(4.2\ K)$ values for all compounds measured are listed in Table 8.

On close observation of the curves around T_t it becomes

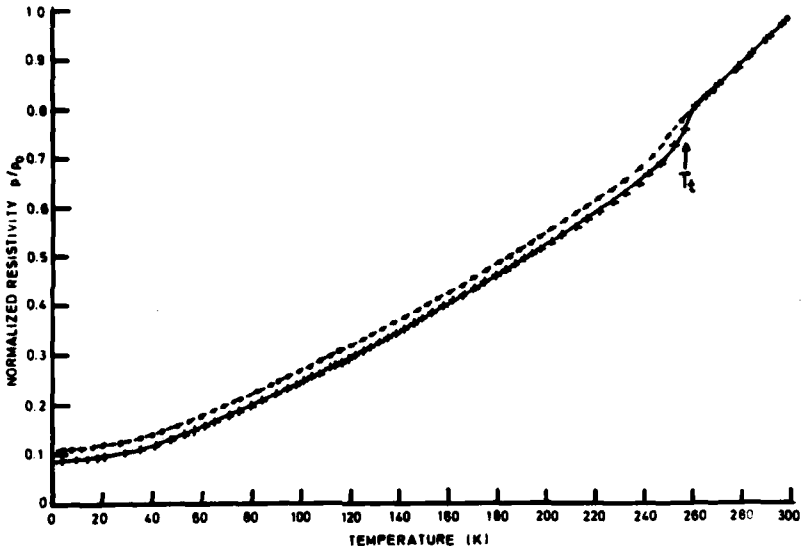

Fig. 48. Normalized resistivity vs. temperature for stage 2 graphite-HNO_3 where ρ_0 is $\rho(T)$ at 300 K(ρ_0 = 3.50 μΩ cm): +, slowly cooled; •, quenched.

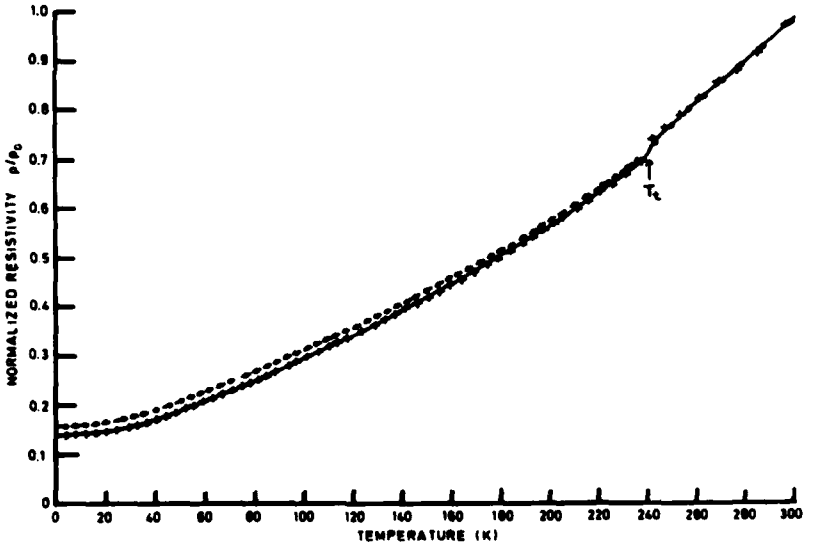

Fig. 49. Normalized resistivity vs. temperature for stage 4 graphite-HNO_3 where ρ_0 is $\rho(T)$ at 300 K(ρ_0 = 4.0 μΩ cm): +, slowly cooled; •, quenched.

apparent that the behavior of graphite-HNO_3 is quite different from that of graphite-SbF_5. The intrinsic temperature dependence (the curve for the slowly cooled specimen), unlike the curve for the quenched specimen, is rather smooth around the T_t value for graphite-SbF_5. However, for graphite-HNO_3, the curves for both the slowly cooled and the quenched specimen have an offset across the T_t value and the effect in the slowly cooled case is even larger than that in the quenched case. The order-disorder transition in graphite-HNO_3 has been shown by x-ray (40), nuclear magnetic resonance (41) and differential scanning calorimetric (42) measurements to be a first-order phase transition. For graphite-SbF_5 the transition is a very broad phase transition which is also supported by the differential scanning calorimetric measurements shown in Fig. 42. T_l and T_u are the lower and upper limits respectively of the transition.

From Table 8 it is evident that T_t for graphite-SbF_5 is more dependent on the stage than T_t for graphite-HNO_3, and $\Delta\rho$ exhibits the same tendency. Both T_t and $\Delta\rho$ indicate either that the charge carriers spread deeper into the graphite layer or, for graphite-SbF_5, that the potential of the intercalant layer has a longer-range influence.

Even though the electronic structure of the acceptor compounds has not been calculated, judging from the band structure of graphite (43), the Fermi surface of the acceptor compounds can be assumed to have cylindrical hole

pockets at the corners of the hexagonal Brillouin zone (30). Kukkonen (44) has extended the electron-phonon scattering theory to semimetals by considering a cylindrical Fermi surface and has predicted a temperature dependence starting at T^5 at low temperatures, going to T^2 and then becoming linear as the temperature increases.

The qualitative analysis of the temperature dependence of resistivity is best understood from the full curves of stage 3 and 4 SbF_5-intercalated graphite (Figs. 40 and 41). Both curves are similar and have four distinct regions.

(1) Below T_A the temperature dependence is slightly higher than T^2.

(2) Between T_A and T_B the curve can be expressed as $\rho = A + BT + CT^2$.

(3) Between T_B and T_C the curve is linear with a slope D.

(4) Above T_C the curve deviates from linear.

The whole curve can be explained consistently by including the cylindrical Fermi surface in the electron-phonon scattering. Because of the high residual resistivity resulting from defects or grain boundary scattering, the T^5 dependence at low temperatures (region (1)) cannot be corroborated. Regions (2) and (3), however, agree well with the T^2 and linear parts of the theory. If only one cylindrical pocket exists, the linear region should extend to room temperature. For our case the interpocket scattering will occur because the phonon wavevector is long enough to connect the carrier pockets at the corners of the hexagonal Brillouin zone. Theoretical

Table 9

Data of the Phase Transition for SbF_5-HOPG and HNO_3 HOPG

	Resistivity measurements			DSC†		EDXD‡
Sample	T_i(K)	T_o(K)	$\Delta\rho$(4.2 K) (10^{-5} Ω-cm)	T_i(K)	T_o(K)	T_i(K)
Stage I SbF_5	185	215	0.393	189	217	185
Stage II SbF_5	180	205	0.0891			
Stage III SbF_5	149	166	0.0599			
Stage IV SbF_5	140	150	0.0479			

†Differential scanning calorimetric.
‡Energy dispersive X-ray diffraction.

calculations of interpocket scattering for high stage C_MK (45) showed that the temperature dependence deviates from linear behavior, which agrees with our results in region (4). The temperatures T_A, T_B and T_C are listed in Table 10. From ref. 44 the temperature T_B is associated with the phonon wavevector that reaches the height of the Fermi cylinder or the Debye wavevector. The smaller T_B for stage 4 is consistent with the longer repeat spacing along the c axis (a longer I_c implies a smaller reciprocal vector along k_c). This suggests that T_B for stages 1 and 2 will be higher, if it can be measured. The temperature T_C is related to the separation of pockets which is caused by the positive charge transfer f from the intercalant layer to the graphite layer. A higher charge transfer will expand the pockets and decrease the distance between pockets, so T_c will be lower. Combining both effects, the absence of a

Table 10

Parameters of the temperature dependence on resistivity for graphite-SbF_5.

Stage	T_A (K)	T_B (K)	T_C (K)	A ($\mu\Omega$ cm)	B ($\mu\Omega$ cm K^{-1})	C ($\mu\Omega$ cm K^{-2})	D ($\mu\Omega$ cm K^{-1})
1	u[a]	u	u	0.408	9.0×10^{-4}	2.9×10^{-5}	u
2	40	u	u	0.278	4.6×10^{-3}	2.1×10^{-5}	u
3	40	140	230	0.333	3.8×10^{-3}	2.2×10^{-5}	0.0072
4	40	130	240	0.317	3.9×10^{-3}	2.1×10^{-5}	0.0068

[a]u, unavailable because there is no linear region.

linear region in stage 1 and 2 compounds (Figs. 38 and 39) can be explained by the hypothesis that the interpocket scattering occurs before the end of the T^2 region. Although detailed analysis requires the phonon spectrum of these compounds, a sufficiently accurate model can be constructed to give us some information about the electronic structure of acceptor compounds. From region (4) it is evident that the temperature dependence of resistivity for interpocket scattering is higher than linear. Thus a further increase in f will lower the onset temperature T_C; this has the reverse effect of lowering the room temperature resistivity. This may explain why the minimum resistivity of graphite intercalation compounds does not occur at stage 1.

The different resistivity values at low temperatures with respect to the slowly cooled and quenched cases can be explained as follows: for most of the acceptor compounds, the intercalant species (at least the neutral one as shown in later sections) are disordered or liquid-like at room temperature, and become ordered below a certain transition

temperature . During the cooling procedure, if insufficient time is allowed for the intercalant species to order, as in the quenched case, the structure of the intercalant layer remains disordered. For the conductive carriers (electrons or holes) in the graphite layer, there will be extra scattering due to the disordered intercalant compared with the ordered case. The possible scattering mechanism could be due to:

(a) The carriers are scattered by the deformation strains in the graphite layers induced by the intercalant

(b) The wave function of the conductive carriers in the graphite layers may have some overlap with the localized wave function of the intercalant. This makes the carriers in the graphite layers sensitive to the in-plane structure of the intercalant layer.

The $\Delta\rho_i$ (T) in the result is related to the extra scattering mechanism induced by the disordered phase.

A possible structure proposed to explain these results is shown in Figure 51. The "X" is the position where the intercalant entity is fixed, while the 'O' is the position where the intercalant entity is quite mobile above T_t. Since the molecules at the 'O' positions are mobile, above T_t the translation distance "X" to "X" (23Å) is the only one observed. As the temperature falls below T_t, there is an extra "O" to "O" or "O" to "X" translation to enhance the peaks at the corresponding energies (d = 5.7 Å). The order-disorder process of the molecules at the "O" positions is the transition that was observed in this compound. The proposed model adequately rationalizes the results listed in Table 9 since

(1) they can only be analyzed as a two-dimensional structure and (2) SbF_5 tends to be polymerized to form chains. For any two-dimensional structure, the peaks should be indexed as the hk0 peaks of that structure, and this is not the case of our data. From the results, it is difficult to tell whether the structure is commensurate or not, because all the peaks are rather broad. Detailed analysis requires more studies on the structure of the intercalant layer with electronic microscope or x-ray diffraction.

With the inter-molecular distance of 5.7Å, an estimate can be made of value of m in C_mSbF_5. Assuming the case of close packing, the value of m is around 11. The real value could be slightly higher, because the intercalant is not perfectly ordered. Otherwise, much stronger intensities for the peaks and a two-dimensional structure should be observed. However, the value of m obtained from the gravimetric measurements was 8.7 (See Table 7). The discrepancy could be explained by supposing that extra SbF_5 molecules were at boundaries and did not account for the structure analysis. In SbF_5-graphite systems, SbF_5 and SbF_6^- were found to act as the intercalant species for SbF_5-intercalated graphite (46, 47, 48). With the assumptions that SbF_5 occupies the "O" position and SbF_6^- at the "X" position in Figure 50 then ionization factor in the well structured area is 25% from the 3 to 1 ratio of the "O" to "X" positions. If the discrepancy between m = 11 and m = 8.7 were included, and it is assumed that extra SbF_5 molecules in the boundaries did not contribute

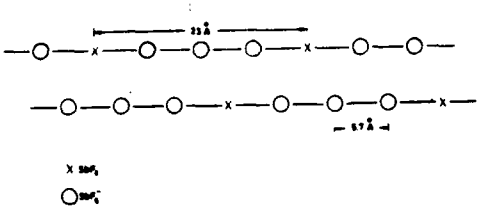

Fig. 50. Proposed in-plane structure for the intercalant layer in SbF_5-HOPG.

to charge transfer, then the ionization factor per intercalant was found to be about 20%. This result agrees with the values obtained from electronic transport measurement. The model as whole consisting of stable SbF_6^- and SbF_5 is supported by an ESCA study of this compound wherein the peak attributable to the SbF_5 could be "pumped off" in a vacuum environment but the SbF_6^- peak remained (48).

E. Conclusion

Reported here are the synthesis techniques for Stage 1-4 SbF_5 intercalated graphite and the measurement of the temperature dependence of resistivity of all four stages. The temperature dependence of resistivity can be explained qualitatively by electron-phonon scattering of the highly anisotropic Fermi surface.

A cooling rate sensitive order-disorder transformation was observed and elucidated with three different experiments: (1) electrical resistivity measurement; (2) DSC measurements and (3) EDXD analysis. All three experiments give very consistent results in the transitions temperature measured, around 185K. The mechanism of the phase transition was attributed to the ordering process of the neutral species in the intercalant layers. From the EDXD analysis, in-plane structure for the intercalant layer for stage one SbF_5-HOPG was proposed. The distance between the ionized intercalant species (SbF_6^-) was measured to be around 23$\mathring{A}$ and the distance between the neutral molecules (SbF_5) was around 5.7$\mathring{A}$.

REFERENCES

1 I.L. Spain, "Chem. and Phys. of Carbon" Vol.8, 1 (1973).

2 T.C. Wu, "Electrical Transport Properties of Graphite Intercalated with Antimony Pentafluoride", Ph.D. Thesis, U. of Pennsylvania (1980).

3 F.L. Vogel, J. Mat. Sci. 12, 982 (1977).

4 W. Rudorff and E. Schulze, Z. Anorg. Allgem. Chem. 277, 156 (1964).

5 F.L. Vogel, G.P. Davis, and S. Mendelsohn, "An Investigation of the Electrical Conductivity of Highly Oriented Graphite Intercalation Compounds", 4th Quarterly Report to Mobility Electronics Research and Development Command, Ft. Belvoir, Virginia 22060 (1980).

6 R. Schlogl, L. Streifinger, R. Pentenrieder, and H.P. Boehm, "Carbon Fluorination by Intercalation of Fluorides in Graphite", Extended Abstracts, 14th Bie-nial Conference on Carbon, American Carbon Society, June 1979, p. 278.

7 M.E. Jacox and D.E. Milligan, J. Chem. Phys., 50, 3252 (1969).

8 D.E. Milligan and M.E. Jacox, J. Chem. Phys., 48, 2265 (1968).

9 C.J. Adams and A.J. Downs, J. Chem. Soc., A, 1534 (1971).

10 G.M. Begun and A.C. Rutenberg, Inorg. Chem., 6, 2212 (1967).

11 J.N. Gan and F.L. Vogel, "Investigation of the Electrical Conductivity of Highly Oriented Graphite Intercalation Compounds", Report to U.S. Army Mobility Equipment Research and Development Command, Ft. Belvoir, Virginia 22060 (1978).

12 "Specification Sheet for #2001 'Superflake' Graphite", Superior Graphite Co. (1980).

13 "Product Data Bulletin for Superflake Purified Natural Crystalline Graphite #2135", Superior Graphite Co. (1981).

14 "Specification Sheet for #4735 Graphite", Superior Graphite Co. (1980).

15 "Calculated Densities of SbF_5-Graphite Compounds", unpublished work.

16 W.D. Ellenson, D. Semmingson, D. Guerard, D.G. Onn and J.E. Fischer, Mat. Sci. Eng. 31, 137 (1977).

17 D. Guerard and A. Herold, Carbon 13, 337 (1975).

18 D. Guerard and A. Herold, C.R. Acad. Sci. 279, 455 (1974).

19 W. Rudorff, Adv. Inorg. Chem. 1, 223 (1959).

20 D.D.L. Chung, G. Dresselhaus and M.S. Dresselhaus, Mat. Sci. Eng. 31 (1977).

21 D.E. Nixon, G.S. Parry and A.R. Ubbelohde, Proc. Roy. Soc. A291, 324 (1966).

22 G.S. Parry, Mat. Sci. Eng. 31, 99 (1977).

23 D.G. Onn, G.M.T. Foley and J.E. Fischer, Mat. Sci. Eng. 31, 271 (1977).

24 A.R. Ubbelohde, Proc. Roy. Soc. A304, 25 (1968).

25 J. Conard and U. Estrade, Mat. Sci. Eng. 31, 173 (1977).

26 L.B. Ebert, R.A. Huggins and J.E. Brauman, Carbon 12, 99 (1974).

27 J. Melin and A. Herold, C.R. Acad. Sci., Ser. C, 280 (1975) 642.

28 G.M.T. Foley, C. Zeller, E.R. Falardeau and F.L. Vogel, Solid State Commun., 24 (1977) 371.

29 T.E. Thompson, E.R. Falardeau and L.R. Hanlon, Carbon, 15 (1977) 39.

30 J.E. Fischer, Electronic properties of graphite intercalation compounds", in F. Levy (ed.), Physics and Chemistry of Materials with Layered Structure, Vol. 6, Reidel, Amsterdam, 1979.

31 C. Zeller, F.L. Vogel and F. Jacques, submitted to Trans. Am. Met. Soc.

32 C. Zeller, A. Denenstein and G.M.T. Foley, Rev. Sci. Instrum., 50 (1979) 602.

33 H.P. Klug and L.E. Alexander, "X-ray Diffraction Procedures for Polycrystalline and Amorphous Materials", 2nd Ed. John Wiley & Son, N.Y. (1974).

34 I.L. Spain, A. R. Ubbelohde and D.A. Young, Philos. Trans. R. Soc. London, 262 (1967) 345.

35 M.E. Potter, Electronic transport properties of stage-one alkali-metal graphite, Master's Thesis, University of Pennsylvania, 1979.

36 Operation Manual of Dupont 990 Thermal Analyzer.

37 A.R. Ubbelohde, Proc. R. Soc. London, Ser. A, 304 (1968) 25.

38 E.J. McRae, J. Melin, H. Fuzellier, J.-F. Mareche and R. Vasse, Proc. 5th London Int. C-nf. on Carbon and Graphite, Vol. 2, Society of Chemical Industry, London, 1978, p. 671.

39 C. Zeller, L.A. Pendrys and F.L. Vogel, J. Mater. Sci., 14 (1979) 2241.

40 A. Avogadro and M. Villa, J. Chem. Phys., 66 (1977) 2359.

41 D.E. Nixon, G.S. Parry and A.R. Ubbelohde, Proc. R. Soc. London, Ser. A, 291 (1966) 324.

42 A. Dworkin and A.R. Ubbelohde, Carbon, 16 (1978) 291.

43 G.S. Painter and D.E. Ellis, Phys. Rev. B, 1 (1970) 4747.

44 C.A. Kukkonen, Phys. Rev. B, 18 (1978) 1849.

45 H. Kamimura, K. Nakao, T. Ohno and T. Inoshita, Electronic structure and properties of alkali-graphite intercalation compounds, to be published.

46 W.C. Forsman, Proceedings of 13th Biennial Conf. on Carbon, p. 153 (1977).

47 W.C. Forsman, D.E. Carl and T. Birchall, to be published.

48 H.A. Resing, F.L. Vogel and T.C. Wu, Mat. Sci. Eng. 41, 113 (1979).

49 "Assuaging the Desire for Swaging the Wire", Steve Mendelsohn, Masters Thesis, University of Pennsylvania, Philadelphia, PA, Dec. 31, 1981.

VII. LIST OF FIGURES

VIII. LIST OF TABLES

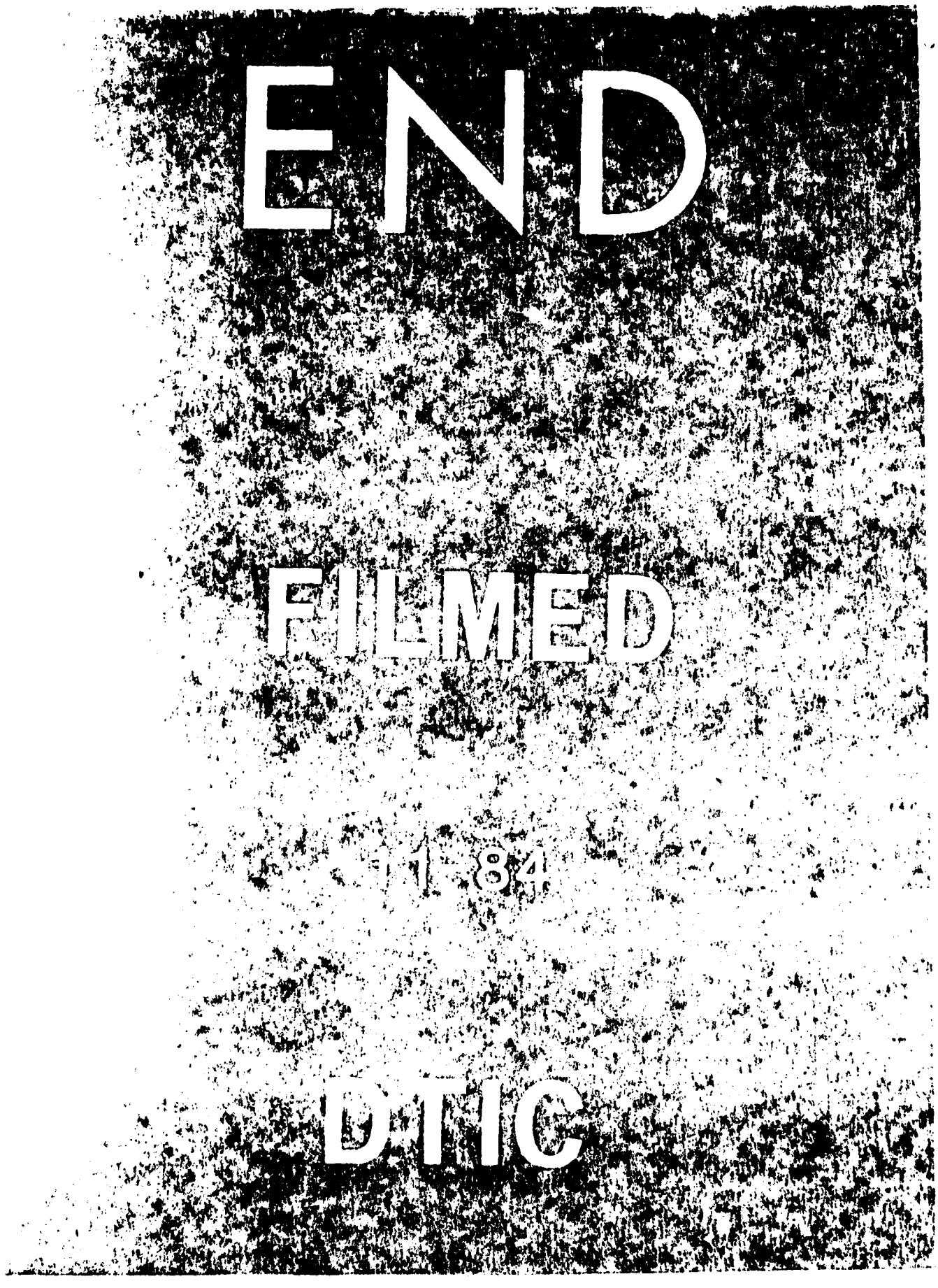
END
FILMED
1-84
DTIC